POD-Based reduced order methods for optimal control problems governed by parametric partial differential equation with varying boundary control

POD-BASED REDUCED ORDER METHODS FOR OPTIMAL CONTROL PROBLEMS GOVERNED BY PARAMETRIC PARTIAL DIFFERENTIAL EQUATION WITH VARYING BOUNDARY CONTROL

MARIA STRAZZULLO[a,*], FABIO VICINI[a,*]

Abstract. In this work we propose tailored model order reduction for varying boundary optimal control problems governed by parametric partial differential equations. With varying boundary control, we mean that a specific parameter changes *where* the boundary control acts on the system. This peculiar formulation might benefit from model order reduction. Indeed, fast and reliable simulations of this model can be of utmost usefulness in many applied fields, such as geophysics and energy engineering. However, varying boundary control features very complicated and diversified parametric behaviour for the state and adjoint variables. The state solution, for example, changing the boundary control parameter, might feature transport phenomena. Moreover, the problem loses its affine structure. It is well known that classical model order reduction techniques fail in this setting, both in accuracy and in efficiency. Thus, we propose reduced approaches inspired by the ones used when dealing with wave-like phenomena. Indeed, we compare standard proper orthogonal decomposition with two tailored strategies: geometric recasting and local proper orthogonal decomposition. Geometric recasting solves the optimization system in a reference domain simplifying the problem at hand avoiding hyper-reduction, while local proper orthogonal decomposition builds local bases to increase the accuracy of the reduced solution in very general settings (where geometric recasting is unfeasible). We compare the various approaches on two different numerical experiments based on geometries of increasing complexity.

1. Introduction

Parametric Optimal Control Problems (OCP($\boldsymbol{\mu}$)s) constrained to parametric partial differential equations (PDE($\boldsymbol{\mu}$)s) are widely used in connection with several engineering applications, such as geothermal and environmental analysis [18, 24, 33, 76, 79], shape optimization [25, 53] or the prediction of fluid flow and transport of contaminants [12, 21, 65]. The main goal of OCP($\boldsymbol{\mu}$)s is to steer the expected behaviour of the PDE($\boldsymbol{\mu}$) towards a desired configuration by means of an external variable, called control. The control acts on the system in order to make the solution as close as possible to the desired state through a PDE($\boldsymbol{\mu}$)-constrained minimization problem. Each parameter $\boldsymbol{\mu} \in \mathcal{P} \subset \mathbb{R}^p$, represents a particular configuration, physical or geometrical, of the controlled system. For each new parameter, a different optimal solution is sought. In the aforementioned applications, OCP($\boldsymbol{\mu}$)s are usually related to time consuming activities where many simulations are required in a small amount of time. This task is not practicable in real-time contexts using standard discretization techniques that feature high computational costs. For these reasons, in recent years, the research proposed different reduced order methods (ROMs) to reduce the total computational effort needed for simulating OCP($\boldsymbol{\mu}$)s, both at steady and time-dependent level [22, 23, 39, 40, 43, 44, 46, 45, 55, 57, 56, 63, 66, 77, 78, 79, 82]. ROMs strategies build a low-dimensional reduced space capable to describe the problem solutions varying with respect to $\boldsymbol{\mu}$ in a reliable and fast way. This approximation is based on the manipulation of some parametric instances of the *high-fidelity* solution, i.e. solutions obtained by a standard discretization, in our case the Finite Element method (FE).

In this work we focus on steady Neumann boundary optimal control problems with a geometrical variation on the control action: the control variable plays a role on a portion of the boundary of the

[a] INdAM research group GNCS member, Italy
* Politecnico of Torino, Department of Mathematical Sciences "Giuseppe Luigi Lagrange", Corso Duca degli Abruzzi, 24, I-10129, Torino, Italy

computational domain and this portion varies according to a specific geometric parameter $\mu_u \in \mathbb{R}$. We are going to address this particular type of OCP($\boldsymbol{\mu}$) as varying boundary OCP($\boldsymbol{\mu}$) (vbOCP($\boldsymbol{\mu}$)). Despite this parametric framework can be exploited to describe complex and interesting physical phenomena, to the best of our knowledge, this is the first time that this model is proposed. As an example, the performances of heat exchangers can be improved by the variation of the baffle geometries, since the heat irradiated from baffles with different lengths has significant effects on the flow characteristics and heat transfer on the shell side [13, 85]. The variation of the baffles seen as boundary controls on the heat exchanger, totally comply with the model at hand. As a further example, the fluid flow inside porous fractured media is strongly influenced by the position and the size of the intersections among the fractures in the rock matrix, thus it is important to characterize the pressure field on each fracture changing the flow injected in the fracture intersections of different length [11, 73]. Fractures moving and intersecting are a natural extension of vbOCP($\boldsymbol{\mu}$)s.

In literature, ROMs for standard geometric OCP($\boldsymbol{\mu}$) have been tackled by means of an affine transformation able to map the desired domain to a corresponding reference shape [47, 71, 72]. However, the affinity hypothesis limits the applicability of the reduction in realistic geometrical configurations. To overcome this problem, non-affine maps were proposed to introduce more complex deformations, [42, 48], coupled with tailored interpolation method to recover the linearity of the bilinear forms of the equations. In this work, we are also interested in exploiting vbOCP($\boldsymbol{\mu}$) on complex domains and shapes, that can hardly be recast in a reference domain. The main novelty of this contribution relies on:

- the proposed vbOCP($\boldsymbol{\mu}$) model, which describes not a single control action but a *varying control action* on the boundary of the considered domain;
- a first experimental analysis for ROMs approaches for vbOCP($\boldsymbol{\mu}$) based on tailored reduced strategies inspired from the ones used in nonlinear model order reduction, i.e. geometric recasting on a reference domain [70] and local bases generation [2, 3, 14, 26, 27, 28, 29, 34, 52].

Indeed, ROMs for vbOCP($\boldsymbol{\mu}$) turned out to be a very difficult task, that features complex parametric behaviour, wave-like-phenomena and non-affine structure. We believe that this work is a first step towards the applications of this model in real-life and interdisciplinary scenarios that naturally fit the proposed framework. We analyzed several reduction techniques and we compare them with standard proper orthogonal decomposition (POD) to propose some guidelines to deal with this peculiar optimal control problem. The comparisons are performed on two numerical tests of increasing geometrical complexity. The final goal is to provide a preliminary numerical investigation to analyze the best approach to be used in different geometrical settings of vbOCP($\boldsymbol{\mu}$)s.

The paper is outlined as follow. In Section 2 we present the vbOCP($\boldsymbol{\mu}$) continuous formulation and its high-fidelity formulation. Section 3 is devoted to introduce ROMs and the tailored reduction techniques needed to deal with vbOCP($\boldsymbol{\mu}$)s. In Section 4 we report the numerical tests in detail. We first test the approaches over a simple geometry and, then, we move our investigation towards more complex computational domains. Conclusions are reported in Section 5.

2. Problem Formulation of vbOCP($\boldsymbol{\mu}$)s

In this section we introduce vbOCP($\boldsymbol{\mu}$)s: i.e. varying boundary OCP($\boldsymbol{\mu}$)s, where the geometrical influence of the control, i.e. the portion of the boundary where the control acts, changes with respect to a parameter. We will focus on linear equations; however, the context can be easily generalized to other PDE($\boldsymbol{\mu}$)s. The discussion follows the formulation presented in other works on steady constrained optimization as [43, 44, 57]. Indeed, even if in this problem the control action is different from standard geometrical OCP($\boldsymbol{\mu}$)s, it totally fits the standard framework.

2.1. Continuous formulation.

Let us consider the parameter $\boldsymbol{\mu} \in \mathcal{P} \subset \mathbb{R}^p$, $p \in \mathbb{N}$: it represents physical and geometrical features of the problem at hand. In our specific setting, the parameter is of the form $(\mu^1, \dots, \mu^{p-1}, \mu_u)$, where $\mu_u \in \mathbb{R}$ determines *where* the boundary control is active. We call Ω an open and bounded regular domain subset of $\mathbb{R}^2$. The portion of the boundary $\partial\Omega$ where Dirichlet conditions apply is Γ_D, while Γ_N is the portion of $\partial\Omega$ where Neumann boundary

conditions are considered. The Neumann boundary is split into $\Gamma_C^{\boldsymbol{\mu}}$, the portion of the boundary where the control acts, and $\Gamma_N^{\boldsymbol{\mu}}$, where homogeneous Neumann conditions are applied. The reason of the dependence on μ_u will be clarified in what follows. Moreover, let $y \in Y_g$ and $u \in U$ be the *state* and the *control* variables of the following spaces

$$Y_g = \{y \in H^1(\Omega) \mid y = g \text{ on } \Gamma_D\} \text{ and } U = L^2(\Gamma_C^{\mu_u}),$$

where $g \in H^{\frac{1}{2}}(\Gamma_D)$ is the value related to the Dirichlet boundary condition. From now on, we will assume $g \equiv 0$, without loss of generality: indeed, the non-homogeneous case can be dealt with a lifting procedure [67]. For the sake of notation, we call $Y = Y_0$. In order to have a meaningful OCP($\boldsymbol{\mu}$), we still need to define, for $\Omega_{\text{obs}} \subset \Omega$, a *desired state* $y_{\text{d}}(\boldsymbol{\mu}) \in L^2(\Omega_{\text{obs}})$. We are interested in the solution of:

$$\min_{(y,u)\in Y\times U} \underbrace{\frac{1}{2}\|y - y_{\text{d}}(\boldsymbol{\mu})\|^2_{L^2(\Omega_{\text{obs}})} + \frac{\alpha}{2}\|u\|^2_U}_{J(y,u;\boldsymbol{\mu})},$$

constrained to a PDE($\boldsymbol{\mu}$) of the following form

$$\begin{cases} D_a(\boldsymbol{\mu})y = f(\boldsymbol{\mu}) & \text{in } \Omega, \\ y = 0 & \text{on } \Gamma_D, \\ \dfrac{\partial y}{\partial n} = u & \text{on } \Gamma_C^{\mu_u}, \\ \dfrac{\partial y}{\partial n} = 0 & \text{on } \Gamma_N^{\mu_u}, \end{cases} \tag{1}$$

where $D_a(\boldsymbol{\mu}) : Y \to Y^*$ is a general differential operator, $f(\boldsymbol{\mu}) \in L^2(\Omega) \subset Y^*$ is an external forcing term and $\alpha > 0$ is a penalization parameter for the control action. As already specified, the boundary *where* the control acts changes with respect to the parameter μ_u, as graphically represented in Figure 1. Namely, the parameter μ_u does not change the shape or the dimension of the domain by means of an affine transformation, but influences the measure of the curves $\Gamma_C^{\mu_u}$ and $\Gamma_N^{\mu_u}$.

Parametric geometrical boundary control was already investigated in several works, see for example [57, 77, 78, 86], but in these cases, the geometrical parameter changes $\Omega := \Omega_\mu$ by means of an affine transformation. Consequently, the related portion of the boundary where the control acts varies, but not its relative measure, as depicted in Figure 2. However, the herein problem is different: the parameter μ_u changes the nature of the problems itself, considering also limit scenarios, where $\Gamma_N^{\mu_u} \to \emptyset$ or $\Gamma_C^{\mu_u} \to \emptyset$. The setting we propose is denoted by the acronym vbOCP($\boldsymbol{\mu}$), as already specified.

The consequences of this framework on the parametric reduction of the model will be widely discussed in the following sections. Let us focus on the problem formulation and the high-fidelity approximation of it. The weak formulation of problem (1) reads: given $\boldsymbol{\mu} \in \mathcal{P}$ find the pair $(y, u) \in Y \times U$ which verifies

$$a(y, q; \boldsymbol{\mu}) = c(u, q; \boldsymbol{\mu}) + \langle G(\boldsymbol{\mu}), q\rangle_{Y^*,Y} \quad \forall q \in Y, \tag{2}$$

where the differential operator $D_a(\boldsymbol{\mu})$ is represented by the bilinear form $a : Y \times Y \to \mathbb{R}$, forcing terms are included in $G(\boldsymbol{\mu}) \in Y^*$ and, $c : U \times Y \to \mathbb{R}$ is defined by:

$$c(u, q; \boldsymbol{\mu}) := \int_{\Gamma_C^{\mu_u}} uq \text{ ds},$$

with $q \in Y$ meant in the sense of traces.
For the sake of notation, we drop the parameter dependence from the variables. Indeed, the value of $\boldsymbol{\mu} \in \mathcal{P}$ affects the optimal solution: namely, $y := y(\boldsymbol{\mu})$ and $u := u(\boldsymbol{\mu})$. We do the same for the desired state, i.e. $y_{\text{d}} := y_d(\boldsymbol{\mu})$.

To state the well-posedness of the problem at hand, we assume that:

(a) $a(\cdot, \cdot; \boldsymbol{\mu})$ is continuous and coercive;
(b) $c(\cdot, \cdot; \boldsymbol{\mu})$ is continuous.

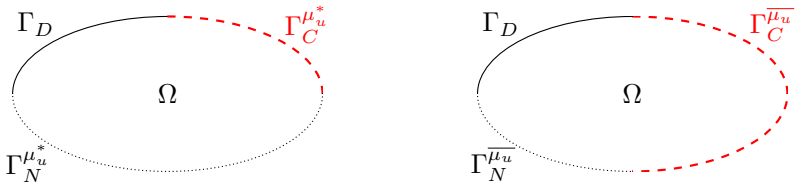

Figure 1. Schematic representation of the computational domain and of the control action of a vbOCP($\boldsymbol{\mu}$) for different values of μ_u, say $\mu_u = \mu_u^*$ (left) and $\mu_u = \overline{\mu_u}$ (right).

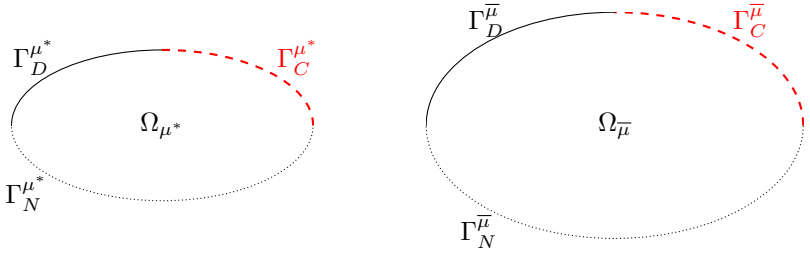

Figure 2. Schematic representation of the computational domain and of the control action of a classical geometrical OCP($\boldsymbol{\mu}$) under affine transformation for different values of μ, say $\mu = \mu^*$ (left) and $\mu = \overline{\mu}$ (right).

Thanks to (a) and (b), given a parameter $\boldsymbol{\mu} \in \mathcal{P}$ and a control $u \in U$, the weak *state equation* (2) is well-posed [67]. Moreover, combining (a) and (b) with the definition of Y and U and $\alpha > 0$, for every parametric instance, we can state the well-posedness of the following *weak minimization problem*:

$$\min\{J(y, u; \boldsymbol{\mu}) : (y, u) \in Y \times U \text{ and } (2) \text{ is verified}\}. \tag{3}$$

To solve (3), we rely on a Lagrangian approach, exploitable since [38, Corollary 1.3] holds under our assumptions. Thus, let us define the *adjoint variable* $p := p(\boldsymbol{\mu}) \in Y$ and the Lagrangian functional as

$$\mathscr{L}(y, u, p; \boldsymbol{\mu}) = J(y, u; \boldsymbol{\mu}) + a(y, p; \boldsymbol{\mu}) - c(u, p; \boldsymbol{\mu}) - \langle G(\boldsymbol{\mu}), p\rangle_{Y^*,Y}.$$

The minimizing pair (y, u) is given by the solution of the following three-equations system: given $\boldsymbol{\mu} \in \mathcal{P}$, find $(y, u, p) \in Y \times U \times Y$ such that

$$\begin{cases} D_y\mathscr{L}(y, u, p; \boldsymbol{\mu})[z] = 0 & \forall z \in Y, \\ D_u\mathscr{L}(y, u, p; \boldsymbol{\mu})[v] = 0 & \forall v \in U, \\ D_p\mathscr{L}(y, u, p; \boldsymbol{\mu})[q] = 0 & \forall q \in Y, \end{cases} \tag{4}$$

which in strong form reads: for a given $\boldsymbol{\mu} \in \mathcal{P}$ find $(y, u, p) \in Y \times U \times Y$ such that

$$\begin{cases} y\chi_{\Omega_{\text{obs}}} + D_a(\boldsymbol{\mu})^* p = y_d \chi_{\Omega_{\text{obs}}} & \text{in } \Omega, \\ \alpha u - p = 0 & \text{in } \Gamma_C^{\mu_u}, \\ D_a(\boldsymbol{\mu}) y = f(\boldsymbol{\mu}) & \text{in } \Omega, \\ \dfrac{\partial y}{\partial n} = u & \text{on } \Gamma_C^{\mu_u}, \\ \dfrac{\partial y}{\partial n} = \dfrac{\partial p}{\partial n} = 0 & \text{on } \Gamma_N^{\mu_u}, \\ y = p = 0 & \text{on } \Gamma_D, \end{cases} \tag{5}$$

where we define $D_a(\boldsymbol{\mu})^*$ as the dual operator of $D_a(\boldsymbol{\mu})$ and $\chi_{\Omega_{\text{obs}}}$ is the characteristic function of Ω_{obs}. The first equation is called *adjoint equation*, the second one *optimality equation* and the third one is the state equation itself. It is clear that, thanks to the equality $\alpha u = p$ on $\Gamma_C^{\mu_u}$ (also in this case, we mean p in the sense of traces), system (5) can be recast in: given $\boldsymbol{\mu} \in \mathcal{P}$, find the pair $(y, p) \in Y \times Y$ such that

$$\begin{cases} y\chi_{\Omega_{\text{obs}}} + D_a(\boldsymbol{\mu})^* p = y_d \chi_{\Omega_{\text{obs}}} & \text{in } \Omega, \\ D_a(\boldsymbol{\mu}) y = f(\boldsymbol{\mu}) & \text{in } \Omega, \\ \dfrac{\partial y}{\partial n} = \dfrac{1}{\alpha} p & \text{on } \Gamma_C^{\mu_u}, \\ \dfrac{\partial y}{\partial n} = \dfrac{\partial p}{\partial n} = 0 & \text{on } \Gamma_N^{\mu_u}, \\ y = p = 0 & \text{on } \Gamma_D. \end{cases} \tag{6}$$

Namely, we consider only two variables and the control is recovered through a postprocessing procedure thanks to the condition $\alpha u - p = 0$ on the control boundary. System (6) can be interpreted in a weak form as follows: given $\boldsymbol{\mu} \in \mathcal{P}$, find $(y, p) \in Y \times Y$ such that

$$\begin{cases} m(y - y_{\text{d}}, w; \boldsymbol{\mu}) + a(w, p; \boldsymbol{\mu}) = 0 & \forall w \in Y, \\ a(y, q; \boldsymbol{\mu}) - \dfrac{1}{\alpha} c(p, q; \boldsymbol{\mu}) = \langle G(\boldsymbol{\mu}), q \rangle_{Y^*, Y} & \forall q \in Y, \end{cases} \tag{7}$$

where $m : Y_{\text{obs}} \times Y_{\text{obs}} \to \mathbb{R}$ is the L^2-inner product restricted to the observation domain.
In the next section, we focus on the discretized version of the problem at hand.

2.2. **High-fidelity formulation.** To deal with system (7), as already specified in the introduction, we use FE as high-fidelity approximation. Let us define a conforming and regular triangulation $\mathcal{T}$ on Ω. Let $Y^{N_h} = Y \cap \mathcal{X}_r$, with

$$\mathcal{X}_r = \{ y \in C^0(\overline{\Omega}) \ : \ y|_K \in \mathbb{P}^r, \ \ \forall K \in \mathcal{T} \},$$

where K is an element of $\mathcal{T}$ and $\mathbb{P}^r$ is the space of polynomials of degree at most r.
Any y^{N_h} and p^{N_h} in Y^{N_h} has a FE expansion of the form

$$y^{N_h} = \sum_1^{N_h} y^i \phi_i, \qquad p^{N_h} = \sum_1^{N_h} p^i \phi_i,$$

where $\{\phi_i\}_{i=1}^{N_h}$ is a basis for Y^{N_h} and y^i, p^i are (unknown) real numbers for $i = 1, \dots, N_h$ (also in this case, we are omitting the $\boldsymbol{\mu}$-dependence of the FE coefficients). We now perform a Galerkin projection in the FE spaces, solving

$$\begin{cases} m(y^{N_h} - y_{\text{d}}, w; \boldsymbol{\mu}) + a(w, p^{N_h}; \boldsymbol{\mu}) = 0 & \forall w \in Y^{N_h}, \\ a(y^{N_h}, q; \boldsymbol{\mu}) - \dfrac{1}{\alpha} c(p^{N_h}, q; \boldsymbol{\mu}) = \langle G(\boldsymbol{\mu}), q \rangle_{Y^*, Y} & \forall q \in Y^{N_h}. \end{cases} \tag{8}$$

Algebraically, we consider $\mathsf{D}_a(\boldsymbol{\mu}) = a(\phi_j, \phi_i; \boldsymbol{\mu})$, for $i, j = 1, \dots, N_h$, as the stiffness matrix. Moreover, $\mathsf{M}_{\text{o}}(\boldsymbol{\mu})$ is the mass matrix related to the L^2-inner product over Ω_{obs} and $\mathsf{C}(\boldsymbol{\mu})_{ij} := c(\phi_j, \phi_i; \boldsymbol{\mu})$, for $i, j = 1, \dots, N_h$ is the control matrix that acts over $\Gamma_C^{\mu_u}$. We denote by $\mathsf{y} \in \mathbb{R}^{N_h}$ and $\mathsf{p} \in \mathbb{R}^{N_h}$

the unknown FE vectors for state and adjoint variables respectively. The same notation is used for the forcing term and the desired state, i.e. $\mathsf{f} = [f^1, \dots, f^{N_h}]^T$ and $\mathsf{y}_\mathrm{d} = [y_\mathrm{d}^1, \dots, y_\mathrm{d}^{N_h}]$ with

$$f^i := \int_\Omega f(\boldsymbol{\mu})\phi_i \, \mathrm{dx} \quad \text{and} \quad y_\mathrm{d}^i := \int_{\Omega_{\mathrm{obs}}} y_\mathrm{d}(\boldsymbol{\mu})\phi_i \, \mathrm{dx}, \ \forall i \in \{1, \dots, N_h\}.$$

The algebraic formulation of the state equation reads

$$\mathsf{D}_a(\boldsymbol{\mu})\mathsf{y} - \frac{1}{\alpha}\mathsf{C}(\boldsymbol{\mu})\mathsf{p} = \mathsf{f}, \tag{9}$$

while the adjoint equation has the following form:

$$\mathsf{M}_\mathrm{o}(\boldsymbol{\mu})\mathsf{y} + \mathsf{D}_a(\boldsymbol{\mu})^T\mathsf{p} = \mathsf{y}_\mathrm{d}. \tag{10}$$

Namely, combining equations (9) and (10), finding the minimizing FE solution $(y^{N_h}, p^{N_h}) \in Y^{N_h} \times Y^{N_h}$ translates in solving the saddle point system

$$\begin{bmatrix} \mathsf{M}_\mathrm{o}(\boldsymbol{\mu}) & \mathsf{D}_a(\boldsymbol{\mu})^T \\ \mathsf{D}_a(\boldsymbol{\mu}) & -\frac{1}{\alpha}\mathsf{C}(\boldsymbol{\mu}) \end{bmatrix} \begin{bmatrix} \mathsf{y} \\ \mathsf{p} \end{bmatrix} = \begin{bmatrix} \mathsf{y}_\mathrm{d} \\ \mathsf{f} \end{bmatrix}. \tag{11}$$

The two-equations system preserves the classical saddle point framework of optimal control problems: indeed, it is well-known that PDE($\boldsymbol{\mu}$) constrained optimization leads to such a peculiar structure both at the steady level [6, 22, 32, 43, 44, 46, 56, 57] and at the time-dependent one [36, 37, 38, 74, 75, 77, 79, 78].

For the well-posedness of the presented saddle point structure, we refer the reader to [10]. We remark that the existence and uniqueness of an optimal solution can be proved by means of Brezzi Theorem [4, 15] as done in [57] for the three-equations system (5). Another proving strategy exploits the Nečas-Babuška theory [54] as done in [78]. Both approaches consider the state and the adjoint solutions in Y^{N_h}. This is the reason why we assumed, from the very beginning, to work with the same space for both variables.

We are now interested in studying vbOCP($\boldsymbol{\mu}$) for several parametric instances: the high-fidelity system is usually not suited to analyze many parameters in a small amount of time. The FE problem suffers the high dimensionality of the optimality system, most of all when the physical phenomenon studied needs fine mesh resolutions. Thus, in the next Sections, we introduce ROMs for vbOCP($\boldsymbol{\mu}$).

3. Reduced Order Methods for vbOCP($\boldsymbol{\mu}$)s

We propose ROMs as a way to reliably solve vbOCP($\boldsymbol{\mu}$)s in a faster way. We introduce the general ideas of this modelling strategy and then we will move towards the algorithms we use to tackle the experiments presented in Section 4. We describe three different approaches to deal with vbOCP($\boldsymbol{\mu}$)s, namely:

- (*Section 3.4*) Proper Orthogonal Decomposition (POD).
- (*Section 3.5*) Local Proper Orthogonal Decomposition (L-POD).
- (*Section 3.6*) Geometric Recasting (Geo-R).

The motivations behind the use of L-POD and Geo-R are discussed in Section 3.2.

3.1. Reduced Problem Formulation.

In this section we describe the basic ideas behind ROM strategies. To make concepts clearer, we explicit the parameter dependence of the variables. Let us consider

$$\mathbb{M} = \{(y(\boldsymbol{\mu}), p(\boldsymbol{\mu})) \mid \boldsymbol{\mu} \in \mathcal{P}\}, \tag{12}$$

as the *solution manifold*, i.e. the set of the optimal solutions varying with respect to the parametric instance. We here assume that $\mathbb{M}$ is smooth with respect to $\boldsymbol{\mu} \in \mathcal{P}$. Once defined a high-fidelity discretization, a *discrete solution manifold* is defined analogously as

$$\mathbb{M}^{N_h} = \{(y^{N_h}(\boldsymbol{\mu}), p^{N_h}(\boldsymbol{\mu})) \mid \boldsymbol{\mu} \in \mathcal{P}\}.$$

Namely, $\mathbb{M}^{N_h} \approx \mathbb{M}$ is a reliable surrogate of $\mathbb{M}$ when the high-fidelity approximation is a good representation of the the continuous model, i.e. when the mesh is fine enough. We now aim at representing the discrete solution manifold by means of a second approximation process: the ROM

approach. The main goal is to rely on a low-dimensional space $Y_N \times Y_N \subset Y^{N_h} \times Y^{N_h} \subset Y \times Y$, with $N \ll N_h$, to solve a smaller system but preserving a certain accuracy in terms of errors between the reduced and the high-fidelity solution. The space Y_N is a linear combination of state and adjoint *snapshots*, i.e. high-fidelity solutions evaluated for properly chosen values of $\boldsymbol{\mu} \in \mathcal{P}$. There are several strategies to build the reduced spaces: we postpone the description of them in the next sections and we now assume to be provided with these reduced spaces. Indeed, once built $Y_N \times Y_N$, we perform a Galerkin projection in the built low-dimensional framework to find the optimal solution for a new parametric instance: given $\boldsymbol{\mu} \in \mathcal{P}$, find $(y_N, p_N) \in Y_N \times Y_N$ such that

$$\begin{cases} m(y_N - y_{\mathrm{d}}, w; \boldsymbol{\mu}) + a(w, p_N; \boldsymbol{\mu}) = 0 & \forall w \in Y_N, \\ a(y_N, q; \boldsymbol{\mu}) - \dfrac{1}{\alpha} c(p_N, q; \boldsymbol{\mu}) = \langle G(\boldsymbol{\mu}), q \rangle_{Y^*,Y} & \forall q \in Y_N. \end{cases} \tag{13}$$

The projection stage is convenient when it is independent from the high-fidelity dimension N_h. To rely on a fast ROM solution, the approach should verify an *offline-online decomposition* that consists in two stages:

- the *offline phase*: the building process and the storing process. It depends on the dimension N_h but it is performed only once;
- the *online phase*: given a new parameter, a Galerkin projection into the low-dimensional framework is performed to provide a solution in a small amount of time.

The aforementioned division is possible only when the problem verifies the *affine decomposition*. In other words, when the weak forms can be written as

$$\begin{aligned} m(\cdot,\cdot;\boldsymbol{\mu}) &= \sum_{l=1}^{Q_m} \Theta_m^l(\boldsymbol{\mu}) m^l(\cdot,\cdot), & a(\cdot,\cdot;\boldsymbol{\mu}) &= \sum_{l=1}^{Q_a} \Theta_a^l(\boldsymbol{\mu}) a^l(\cdot,\cdot), \\ c(\cdot,\cdot;\boldsymbol{\mu}) &= \sum_{l=1}^{Q_c} \Theta_c^l(\boldsymbol{\mu}) c^l(\cdot,\cdot), & \langle G(\boldsymbol{\mu}), q \rangle &= \sum_{l=1}^{Q_G} \Theta_G^l(\boldsymbol{\mu}) \langle G^l, q \rangle_{Y^*,Y}, \end{aligned} \tag{14}$$

for some Q_m, Q_a, Q_c and Q_G in $\mathbb{N}$, with $\Theta_m^l, \Theta_a^l, \Theta_c^l$, and Θ_G^l smooth real functions depending on $\boldsymbol{\mu}$ and $m^l(\cdot,\cdot), a^l(\cdot,\cdot), c^l(\cdot,\cdot)$ and $\langle G^l, \cdot \rangle_{Y^*,Y}$ independent of $\boldsymbol{\mu}$. The structure (14) is necessary to rely on an offline-online concept. In this way, in the offline stage we can assemble and store all the $\boldsymbol{\mu}$-independent quantities together with the reduced spaces basis functions, while, in the online phase, we compute the $\boldsymbol{\mu}$-dependent quantities for a specific parametric instance and the reduced optimality system is assembled and solved.
In our context, this assumption does not hold. Indeed, the bilinear form $c(\cdot,\cdot;\boldsymbol{\mu})$ does not admit an affine decomposition, since the boundary integration over $\Gamma_C^{\mu_u}$ changes at each $\boldsymbol{\mu}$ and it has to be assembled for each parameter.
In order to recover the affine assumption, one can rely on several techniques, such as Empirical Interpolation Method (EIM) or Discrete Empirical Interpolation Method (DEIM). We refer the interested reader to [8, 20] and [35, Chapter 5]. We stress that in some of the results we are going to present in Section 4, we exploited DEIM to guarantee offline-online decomposition and, consequently, computational efficiency. We briefly recall DEIM process in Section 3.3.

3.2. **The rational behind tailored reduced strategy for vbOCP($\boldsymbol{\mu}$).** We observe from the numerical simulations of Section 4.1, that the solution drastically changes with respect to μ_u and the problem might feature very complicated structures as transport-wave-like phenomena, i.e. moving fronts. The detail are described in Section 4, together with the test cases.

Namely, when dealing with vbOCP($\boldsymbol{\mu}$), standard reduced approaches may lead to inefficient reduced solution. Indeed, vbOCP($\boldsymbol{\mu}$)s need many basis functions to provide and accurate representation of the high-fidelity approximation. A large number of modes, combined with the non-affine structure of the problem, translates into unbearable reduced simulations, i.e. the reduced model is not competitive with respect to the high-fidelity one.

For this reason we decide to exploit strategies that are usually related to the field of nonlinear manifold reduction. In the last years, many approaches have been conceived to solve this kind

of issues and much effort has been done to develop techniques capable to decrease the number of basis functions needed to efficiently reduce the system. They rely on pre-processed snapshots before applying the reduction algorithm [41, 59, 58, 61, 68, 80] or on adapting the bases to the moving features [62, 87]. Other approaches employ a transformation map of the solution in a reference domain to avoid the nonlinear features of the solution manifold, we refer the interested reader to [17, 59, 81] and the reference therein. These strategies have been successfully employed for advection-dominated phenomena, most of all in a time-dependent setting.

Other strategies build local reduced basis since global structure may lead to inaccurate results if few modes are exploited. We postpone the discussion on local ROMs to Section 3.5. Here, we report a far from exhaustive list of useful references on the topic [2, 3, 14, 26, 27, 28, 29, 34, 52].

Moreover, we want to stress that a novel and successful research field focuses on the use of ROMs enhanced by artificial intelligence techniques to deal with nonlinear model order reduction, the interested reader may refer to [30, 31, 49, 69] and the reference therein.

3.3. **DEIM.** The DEIM approach overcomes the problem of dealing with a non-affine system, as in our case. We follow the seminal paper [20]. We approximate the bilinear form $c(\cdot,\cdot,\boldsymbol{\mu})$ applying a projection onto a subspace of dimension $N_{DEIM} \ll N_h$. We recall that the bilinear form related to the control is:

$$c(u,q;\boldsymbol{\mu}) = \int_{\Gamma_C^{\mu_u}} uq \,\mathrm{ds} = \int_{\Gamma_C^0} \chi_{\mu_u} uq \,\mathrm{ds},$$

where $\chi_{\mu_u} = 1$ where the control is applied and $\chi_{\mu_u} = 0$ elsewhere, while $\Gamma_C^0 \subset \partial\Omega$ is the maximum portion of the boundary that can feature the control action. All the quantities are meant in the sense of traces. To apply the DEIM algorithm, we consider a discrete version of χ_{μ_u}, i.e. $\boldsymbol{\chi}_{\mu_u} \in \mathbb{R}^{N_h}$: the FE coefficient array. The goal is to approximate the characteristic function $\boldsymbol{\chi}_{\mu_u}$ as

$$\overline{\boldsymbol{\chi}}_{\mu_u} = \sum_{q=1}^{N_{DEIM}} \Theta^q(\boldsymbol{\mu}) \mathsf{z}_q, \tag{15}$$

with $\mathsf{z}_q \in \mathbb{R}^{N_h}$ basis vectors that do not depend on the parameter and $\Theta^q(\boldsymbol{\mu})$ are real coefficients for each value of the parameters. The basis vectors $\{\mathsf{z}_q\}_{q=1}^{N_{DEIM}}$ are built through a POD approach over the evaluation of several instances of $\boldsymbol{\chi}_{\mu_u}$.

We call the basis matrix related to the DEIM approximation as

$$\mathsf{Z}^{DEIM} = [\mathsf{z}_1, \ldots, \mathsf{z}_{N_{DEIM}}].$$

Algebraically, (15) can be written as

$$\overline{\boldsymbol{\chi}}_{\mu_u} = \mathsf{Z}^{DEIM} \Theta(\boldsymbol{\mu}),$$

where $\Theta(\boldsymbol{\mu}) = [\Theta^1(\boldsymbol{\mu}), \ldots, \Theta^{N_{DEIM}}(\boldsymbol{\mu})]^T$ is the column vector of the coefficients. To complete the offline procedure we need to find a set of interpolation indices $\mathbb{I} \subseteq \{1, \ldots, N_h\}$ which will be used in the online phase to find the specific coefficients $\Theta^q(\boldsymbol{\mu}^*)$ for a given $\boldsymbol{\mu}^* \in \mathcal{P}$. The set $\mathbb{I}$ is computed by the magic point algorithm, see e.g. [9, 51].

In the online phase, for a specific parameter $\boldsymbol{\mu}^*$, we select the N_{DEIM} rows given by the indices in $\mathbb{I}$ to determine the coefficient $\Theta(\boldsymbol{\mu}^*)$. Thus, defining the matrix

$$\mathsf{P} = [\mathsf{e}^{\mathbb{I}_1}, \ldots, \mathsf{e}^{\mathbb{I}_{N_{DEIM}}}] \in \mathbb{R}^{N_h} \times \mathbb{R}^{N_{DEIM}},$$

where $\mathsf{e}^{\mathbb{I}_i} \in \mathbb{R}^{N_h}$, $\mathsf{e}_j^{\mathbb{I}_i} = \delta_{ij}$ and δ_{ij} stays for the Kronecker delta, the vector $\Theta(\boldsymbol{\mu})$ can be found solving the following system:

$$\mathsf{P}^T \boldsymbol{\chi}_{\mu_u} = (\mathsf{P}^T \mathsf{Z}^{DEIM}) \Theta(\boldsymbol{\mu}).$$

Namely,

$$\overline{\boldsymbol{\chi}}_{\mu_u} = \mathsf{Z}^{DEIM} \Theta(\boldsymbol{\mu}) = \mathsf{Z}^{DEIM} (\mathsf{P}^T \mathsf{Z}^{DEIM})^{-1} \mathsf{P}^T \boldsymbol{\chi}_{\mu_u}.$$

Once we are provided of this representation, the affine structure of the problem is recovered and the online-offline paradigm holds.

In the numerical results of Section 4, we will see the benefits of enhancing ROMs by DEIM technique.

3.4. **POD.** We focus on the building process based on POD-Galerkin strategy. The interested reader may refer to [16, 19, 35] for a detailed discussion on this algorithm. We here summarize the main features of it together with its generalization to OCP($\boldsymbol{\mu}$)s (that it is suited for vbOCP($\boldsymbol{\mu}$), too). We start sampling $(\boldsymbol{\mu}_1, \dots, \boldsymbol{\mu}_{N_{\max}}) \in \mathcal{P}$ and computing the related high-fidelity approximations

$$(y^{N_h}(\boldsymbol{\mu}_1), \dots, y^{N_h}(\boldsymbol{\mu}_{N_{\max}}) \text{ and } (p^{N_h}(\boldsymbol{\mu}_1), \dots, p^{N_h}(\boldsymbol{\mu}_{N_{\max}}).$$

From now on, we describe the process for the state variable only, since we apply a separate POD for the two variables: the procedure repeats for the adjoint variable, analogously.
We aim at building $N < N_{\max}$ basis functions by means of snapshots manipulation, to discard redundant information from the sampled parametric solutions.
We assume that the number of samples $N_{\max}$ is large enough to well represent the solution manifold (12). The process provides the $N-$dimensional reduced space Y_N^y (and not Y_N) that minimizes the following quantities:

$$\sqrt{\frac{1}{N_{\max}} \sum_{i=1}^{N_{\max}} \min_{\zeta_N \in Y_N^y} \|y^{N_h}(\boldsymbol{\mu}_i) - \zeta_N\|_Y^2}.$$

To reach the minimization goal, we define the correlation matrix $\mathbf{C}^y \in \mathbb{R}^{N_{\max} \times N_{\max}}$ of state snapshots and we solve the eigenvalue problem $\mathbf{C}^y \omega_n^y = \lambda_n^y \omega_n^y$ for $1 \le n \le N_{\max}$, with $\|\omega_n^y\|_Y = 1$. Due to the definition of correlation matrix, we can order the all-positive eigenvalues as $\lambda_1^y > \dots > \lambda_{N_{\max}}^y > 0$ and retain the first N eigenpairs $(\lambda_n^y, \omega_n^y)$ for $1 \le n \le N$. Finally, the basis are built as [35, 64], i.e.

$$\xi_n^y = \frac{1}{\sqrt{\lambda_n^y}} \sum_{m=1}^{N_{\max}} (\omega_n^y)_m y^{N_h}(\boldsymbol{\mu}_m), \qquad 1 \le n \le N. \tag{16}$$

The choice of $N_{\max}$ and N can be made by studying the behaviour of λ_n^y for $1 \le n \le N_{\max}$. Indeed, defining as $P_N : Y \to Y_N^y$ the projector from Y onto Y_N^y, the following relation holds [35, 64]:

$$\sqrt{\frac{1}{N_{\max}} \sum_{i=1}^{N_{\max}} \|y^{N_h}(\boldsymbol{\mu}_i) - P_N(y^{N_h}(\boldsymbol{\mu}_i))\|_Y^2} = \sqrt{\sum_{i=N+1}^{N_{\max}} \lambda_m^y}. \tag{17}$$

Namely, a fast decay of the eigenvalue magnitude guaratees a good representation of the high-fidelity solution with a few basis functions.
The application of the POD to the adjoint variable leads to another reduced space Y_N^p. In principle, it can be different from Y_N^y and this does not guarantee the well-posedness of the problem as proposed in Section 2.2. Thus, we need a post-processing step over the basis. We apply the *aggregated space* technique to build a common space for state and adjoint, a standard approach when dealing with OCP($\boldsymbol{\mu}$)s, see e.g. [5, 6, 22, 32, 43, 44, 56, 57, 66] as references.
The final reduced space is of the form

$$Y_N = \{(\xi_n^y, \xi_n^p),\ n = 1, \dots, N\}.$$

In this way, we can define the basis matrix $\mathsf{Q} = [\xi_1^y, \cdots, \xi_N^y, \xi_1^p, \cdots, \xi_N^p] \in \mathbb{R}^{N_h \times 2N}$ and employ a Galerkin projection over the high-fidelity quantities of (11) we stored in the offline phase, dealing with a $4N \times 4N$ system of the form

$$\begin{bmatrix} \mathsf{M}_N & \mathsf{D}_N^T \\ \mathsf{D}_N & \mathsf{C}_N \end{bmatrix} \begin{bmatrix} \mathsf{y}_N \\ \mathsf{p}_N \end{bmatrix} = \begin{bmatrix} \mathsf{y}_{\mathrm{d}N} \\ \mathsf{f}_N \end{bmatrix}, \tag{18}$$

where $\mathsf{M}_N = \mathsf{Q}^T M_{\mathrm{o}}(\boldsymbol{\mu})\mathsf{Q}$, $\mathsf{D}_N = \mathsf{Q}^T \mathsf{D}_a(\boldsymbol{\mu})\mathsf{Q}$, $\mathsf{C}_N = \mathsf{Q}^T \mathsf{C}(\boldsymbol{\mu})\mathsf{Q}$, $\mathsf{y}_{\mathrm{d}N} = \mathsf{Q}^T \mathsf{y}_{\mathrm{d}N}$ and $\mathsf{f}_N = \mathsf{Q}^T \mathsf{f}$. We stress that if the affine decomposition holds, the high-fidelity matrices inherit the affine property from their continuous counterpart (14) and the reduced $\boldsymbol{\mu}$-independent part of the matrices can be stored once and for all in the offline phase.

3.5. **L-POD.** To increase the accuracy of the reduced order model, the sampled solution manifold $\mathbb{M}^{N_h}$ is divided into different *snapshot regions* and for each region a reduced model is built. The idea of local POD is not new in literature. Indeed, building separate sets of basis functions for a subspace of the parametric solution manifold turns out to be beneficial to reduce the dimensionality of complicated problems. The interested reader may refer to several papers, such as [2, 3, 14, 26, 27, 28, 29, 34, 52]. Local reduced order modelling has been successfully employed in many fields of applications, for example in cardiac models [60, 84], computational fluid dynamics and aerodynamics [83]. The accuracy of the local bases is higher with respect to a global approach when one is dealing with nonlinear and non-affine problems. Let us assume to have clustered the N_{max} snapshots (we postpone the discussion on *how cluster them* later on) in J groups. In this way, we divide $\mathbb{M}^{N_h}$ in sub-regions $\{\mathbb{M}_i^{N_h}\}_{i=1}^J$ and we want to separately reconstruct the local solution manifolds $\mathbb{M}_i^{N_h}$ for $i = 1, \dots, J$. The new offline phase consists in the application of the POD strategy enhanced with aggregated spaces for each of the sub-manifold. This translates in J basis matrices Q_i for $i = 1, \dots, J$, that are able to locally represent the system. Indeed, the online procedure first sorts a specific parameter, say $\boldsymbol{\mu}^*$, into a group and, then, applies the specific POD-Galerkin procedure over the selected local space.

Algorithm 1 Pseudo-code for L-POD (Offline phase)

$N_{\max}, N, \tau$, LIST $= [I_{\mu_u}], M, i = 0, [\boldsymbol{\mu}_1, \cdots, \boldsymbol{\mu}_{N_{\max}}], J = 0$ ▷ Inputs
for $\boldsymbol{\mu} \in [\boldsymbol{\mu}_1, \cdots, \boldsymbol{\mu}_{N_{\max}}]$ **do**
    Solve (11) and store $y(\boldsymbol{\mu})$ and $p(\boldsymbol{\mu})$
end for
while LIST $\neq \emptyset$ or $i < M$ **do**
    for $I \in LIST$ **do**
        LIST = LIST$\backslash I$
        for $\mu_u \in [\mu_{u1}, \cdots, \mu_{uN_{\max}}]$ **do**
            if $\mu_u \in I$ **then**
                Enrich local state and adjoint covariance matrices
            end if
        end for
        Solve the $N-$eigenvalue problem over the local covariance matrices
        if $\lambda_N^y > \tau$ **then**
            $i = i + 1$
            Halve I in I_1 and I_2
            LIST = LIST $\cup\, I_1 \cup I_2$
        else
            $J = J + 1$
            Build the local $N-$dimensional basis (aggragated spaces)
            Build the local reduced operators
        end if
    end for
end while

It remains to understand how to cluster the snapshots and how to sort the online parameters. In literature, many strategies have been employed. For time dependent problems, a classical approach is to divide the considered time interval in time windows and build a reduced space for each one of them, as done in [14, 26, 27]. Another strategy relies on the division of the parametric space $\mathcal{P}$ adaptively, see e.g. [28, 29, 34]. Last, one can use classification algorithms to cluster the snapshots in a beneficial way, as done in [60].
We propose a tailored algorithm for this specific problems, guided by the numerical results we are going to show in Section 4.
As we already specified in Section 3.2, the change of μ_u plays a crucial role in the complexity of the

problem. Thus, our choice was to adaptively divide the geometrical parameter interval I_{μ_u}, where μ_u lives. First of all, we fix a tolerance τ, a maximum value of divisions M and a basis number N. We applied a first POD on the whole interval I_{μ_u} for a given basis number N. If the state eigenvalue $\lambda_N^y \geq \tau$, we halve I_{μ_u} in $I_{\mu_u}^1$ and $I_{\mu_u}^2$. We proceed analogously for the two sub-intervals. If the criterion is verified we stop. If not, we continue halving once again the interval we are dealing with. The procedure ends when all the intervals meet the criterion, or when I_{μ_u} is divided in M sub-intervals. This procedure leads to a partition of the geometrical parametric interval as

$$I_{\mu_u} = \bigcup_{i=1}^{J} I_{\mu_u}^i,$$

and to the creation of J reduced spaces, one for each of the sub-intervals, with $J \leq M$. Summing up, in the offline phase:

- we generate all the high-fidelity solutions and we apply a first POD;
- if the criterion over λ_N^y is not verified, we halve I_{μ_u} and we separate the snapshots, consequently. We perform the POD operation on each sub-interval. We iteratively repeat this process;
- when we meet the criterion over λ_N^y for a sub-interval, we build and store the local basis functions.

If the tolerance on the state eigenvalues is not reached, the procedure stops after a maximum number of iterations.
In the online phase, it suffices to sort $\boldsymbol{\mu}$ with respect to the sub-interval it belongs to. We recap the offline procedure in Algorithm 1. We took inspiration from the time-windowed strategies presented in [14, 26, 27] adapting them to the vbOCP($\boldsymbol{\mu}$). We recall that the partition of I_{μ_u} looks a natural choice, since the transport phenomena are directly related to μ_u, as we will discuss in Section 4.

Remark 1. *The strategy we propose is only one path one can take to build local spaces. We believe that many different adaptive strategies, even more efficient, can be found to deal with vbOCP($\boldsymbol{\mu}$), as we stressed out in the beginning of this section. However, our goal is to underline the main features of the vbOCP($\boldsymbol{\mu}$) model as a first step towards a more complete and deeper analysis. Thus, we did not try other techniques since such an experimental study is beyond the scope of the contribution. Furthermore, we stress that the adaptive strategy is only related to the geometrical parameter interval I_{μ_u}. The extension to three-dimensional (3D) problem is natural, since the vbOCP($\boldsymbol{\mu}$) can be represented by a characteristic function $\chi_{\mu_u}(x_1, x_2, x_3)$, where x_i for $i = 1, 2, 3$ denotes the coordinates of the domain Ω.*

3.6. **Geo-R.** When dealing with simple settings, it is possible to recast the problem as formulated in [70]. The strategy, in the standard OCP($\boldsymbol{\mu}$) framework, was already exploited in several works, see e.g. [7, 56, 57, 77, 78]. The aim is to solve the optimality FE systems (8) and the reduced one (13) in a reference domain $\Omega_o := \Omega(\mu_u^o)$. In our case, this means to recast the problem in a framework where the control boundary and, consequently, the Neumann boundary, are "fixed", simplifying the setting at hand. In the following, we indicate with $\mathring{\Xi}$ and $\overline{\Xi}$ the internal part and the closure of a spatial domain Ξ, respectively.
We assume that the domain Ω_o is the union of R non-overlapping subdomains Ω_o^r, i.e.

$$\Omega_o = \bigcup_{r=1}^{R} \Omega_o^r \text{ with } \mathring{\Omega}_o^{r'} \cap \mathring{\Omega}_o^{\bar{r}} = \emptyset \text{ for } 1 \leq r' < \bar{r} \leq R. \tag{19}$$

The same assumption holds true for the domain Ω, i.e.

$$\Omega = \bigcup_{r=1}^{R} \Omega^r \text{ with } \mathring{\Omega}^{r'} \cap \mathring{\Omega}^{\bar{r}} = \emptyset \text{ for } 1 \leq r' < \bar{r} \leq R. \tag{20}$$

We want to define a piece-wise affine map $T_{\mu_u} : \Omega_o \to \Omega$ such that $\Omega = T_{\mu_u}(\Omega_o)$. The map T_{μ_u} is made by local maps $T_{\mu_u}^r$ defined over the subdomains Ω_o^r and on each subdomain $T_{\mu_u}^r$ is invertible.

We remark the $T^r_{\mu_u}(\Omega^r_o) = \Omega^r$. Moreover, the local maps glue continuously, namely, given a point $\mathbf{x} \in \Omega_o$:

$$T^{r'}_{\mu_u}(\mathbf{x}_o) = T^{\bar{r}}_{\mu_u}(\mathbf{x}_o) \quad \forall \mathbf{x}_o \in \overline{\Omega}^{r'}_o \cap \overline{\Omega}^{\bar{r}}_o, \text{ for } 1 \le r' < \bar{r} \le R. \tag{21}$$

The last assumption is that the local maps are affine transformations. Indeed, for every $r = 1, \dots, R$ we require $T^r_{\mu_u}(\mathbf{x}_o) = \mathsf{c}^r(\mu_u) + \mathsf{G}^r(\mu_u)\mathbf{x}_o$, where $\mathsf{c}^r(\mu_u) \in \mathbb{R}^2$ is a translation vector and $\mathsf{G}^r(\mu_u) \in \mathbb{R}^{2\times 2}$ is a linear transformation matrix. Once defined the map, it is clear that the continuous version of the optimality system (7), together with the FE one (8) and the reduced one (13), can be solved in the new reference domain after a change of variables over the integral forms using the inverse of the local maps. We refer the reader to [70] for the details. As already specified, the main advantage is that we work with a reference $\Gamma^{\mu_u^o}_C$, i.e. all the snapshots are taken in a new framework where the control boundary stays unchanged. Once the change of variable is performed, one can proceed with standard ROM techniques, as POD. Once the map is found, after the change of variable problem (7) becomes: given $\boldsymbol{\mu} \in \mathcal{P}$, find $(y, p) \in Y \times Y$ such that

$$\begin{cases} \overline{m}(y - y_{\mathrm{d}}, w; \boldsymbol{\mu}) + \overline{a}(w, p; \boldsymbol{\mu}) = 0 & \forall w \in Y, \\ \overline{a}(y, q; \boldsymbol{\mu}) - \dfrac{1}{\alpha}\overline{c}(p, q; \boldsymbol{\mu}) = \langle \overline{G}(\boldsymbol{\mu}), q\rangle_{Y^*,Y} & \forall q \in Y, \end{cases} \tag{22}$$

where $Y = H^1_0(\Omega_o)$ is this framework.

4. Numerical Results

In this section we present two different tests over different geometries. The governing PDE($\boldsymbol{\mu}$) is an advection-diffusion equation for both the experiments. The problem reads: given $\boldsymbol{\mu} \in \mathcal{P}$, find the pair $(y, p) \in Y \times Y$ such that

$$\begin{cases} y\chi_{\Omega_{\mathrm{obs}}} - \dfrac{1}{\mu_1}\Delta p - x_2(1-x_2)\dfrac{\partial p}{\partial x_1} = \mu_2\chi_{\Omega_{\mathrm{obs}}} & \text{in } \Omega, \\ -\dfrac{1}{\mu_1}\Delta y + x_2(1-x_2)\dfrac{\partial y}{\partial x_1} = 0 & \text{in } \Omega, \\ \dfrac{1}{\mu_1}\dfrac{\partial y}{\partial n} = 0 & \text{on } \Gamma^{\mu_u}_N, \\ \dfrac{1}{\mu_1}\dfrac{\partial p}{\partial n} + x_2(1-x_2)n_1 p = 0 & \text{on } \Gamma^{\mu_u}_N, \\ \dfrac{1}{\mu_1}\dfrac{\partial y}{\partial n} = \dfrac{1}{\alpha}p & \text{on } \Gamma^{\mu_u}_C, \\ y = 1 \text{ and } p = 0 & \text{on } \Gamma_D, \end{cases} \tag{23}$$

where (x_1, x_2) denotes the spatial coordinates of the domain Ω and n_1 is the first component of the outer vector to $\Gamma^{\mu_u}_N$. We also refer to the vector of spatial coordinates as $\mathbf{x} := [x_1, x_2]^T$.
We recall that, despite the same constraint, the geometry of the test cases drastically changes. This is the key aspect of the numerical results we are going to show: for standard and simple geometries the problem simplifies and reference-domain-based techniques can be exploited in order to achieve satisfactory results. This is not the case for complex geometries (nonlinear boundaries, holes...), where these techniques can be hardly applied.

4.1. Test Case 1: POD, L-POD and Geo-R over a standard geometry.

We propose a vbOCP($\boldsymbol{\mu}$) governed by (23) with two physical parameters and the control boundary that changes with respect to μ_u, as depicted in Figure 3. The observation domain is $\Omega_{\mathrm{obs}} = \Omega_3 \cup \Omega_4$ where $\Omega_3 = [1, 2] \times [0.8, 1]$, $\Omega_4 = [1, 2] \times [0, 0.2]$, while Ω_1 is the unit square and $\Omega_2 = [1, 2] \times [0.2, 0.8]$. The control acts on the boundary $\Gamma^{\mu_u}_C = ([1 + \mu_u, 2] \times \{0\}) \cup ([1 + \mu_u, 2] \times \{1\})$. Also the portion of the domain where Neumann boundary conditions are applied changes with respect to μ_u: $\Gamma^{\mu_u}_N = ([1, 1 + \mu_u) \times \{0\}) \cup ([1, 1 + \mu_u) \times \{1\}) \cup (\{2\} \times [0, 2])$.

The parameter is $\boldsymbol{\mu} := (\mu_1, \mu_2, \mu_u) \in \mathcal{P} = (6.0, 20.0) \times (0.5, 3.0) \times (0.0, 1.0)$, where μ_1 is related to the Péclet number, μ_2 describes the constant desired state we want to reach in Ω_{obs} and μ_u,

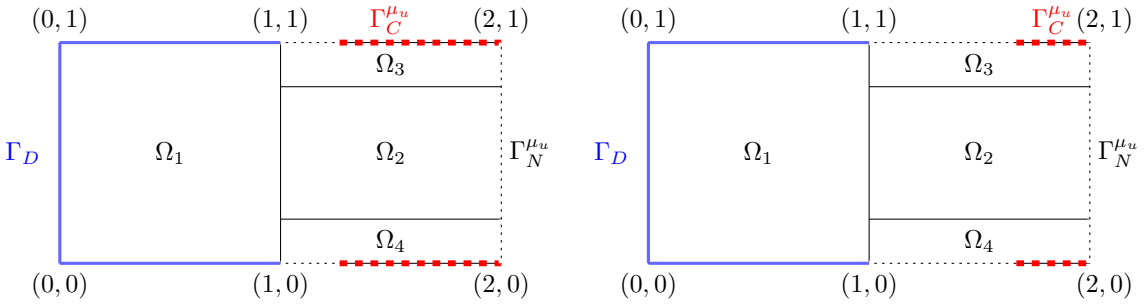

Figure 3. (Test 1). Domain Ω. *Observation domain:* $\Omega_{\text{obs}} = \Omega_3 \cup \Omega_4$, *Control domain:* $\Gamma_C^{\mu_u}$ (red dashed line). *Blue solid line:* Dirichlet boundary conditions. *Black dotted line:* Neumann boundary conditions. We represent the domain for $\mu_u = 0.3$ (left) and $\mu_u = 0.7$ (right).

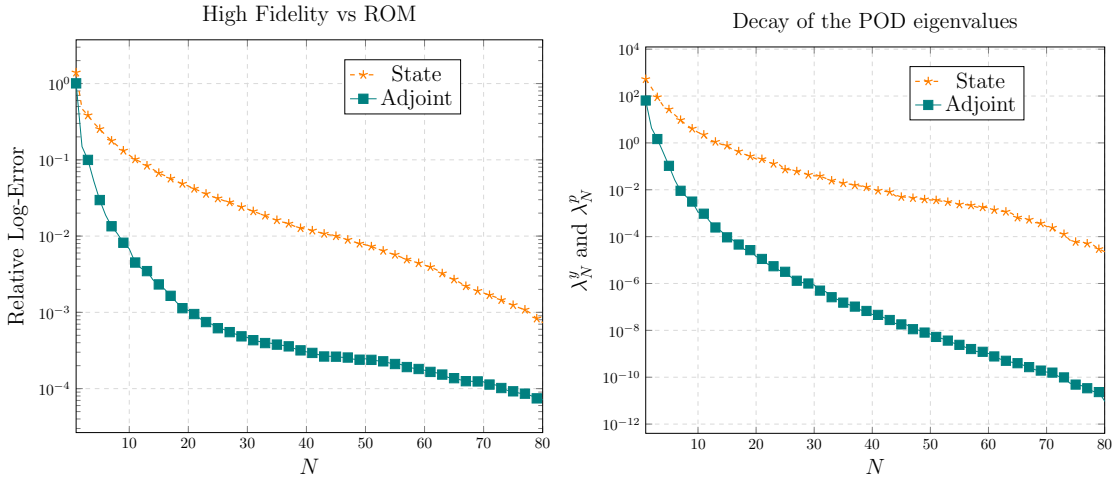

Figure 4. (Test 1: POD). *Left.* Averaged relative log-error for the two variables. *Right.* Decay of the eigenvalues for the two variables.

as already specified, changes the boundary portion where the control acts. In analogy with the numerical results shown in [44, 57, 77, 78], we choose $\alpha = 0.07$. We now describe the performances of standard POD.

First of all, we recover the affine decomposition through a DEIM approach applied to a training set of 350 uniformly distributed parameters. The method stops when the DEIM approximation is a good representation of the actual problem (the stopping criterion over the eigenvalue decay is set to be lower then 10^{-5} and leads to $N_{DEIM} = 80$). Thus, a standard POD is performed on other 300 snapshots picked by means of uniform distribution. The high-fidelity dimension of the $\mathbb{P}^1 - \mathbb{P}^1$ approximation is $2N_h = 10366$. In Figure 4 (left plot) we show the averaged relative errors for the state and the adjoint variable between the high-fidelity and reduced solutions. We plot the average value over a testing set of 150 uniformly distributed parameters in $\mathcal{P}$ of the quantities

$$e_y = \frac{\|y^{N_h} - y_N\|_Y}{\|y^{N_h}\|_Y} \quad \text{and} \quad e_p = \frac{\|p^{N_h} - p_N\|_Y}{\|p^{N_h}\|_Y}.$$

We denote these averaged quantities with E_y and E_p, respectively. It is clear that, too many basis functions are needed in order to reach acceptable values for E_y, say $N = 80$ to reach $E_y \sim O(10^{-3})$. We remark that $N = 80$ translates in a reduced system of dimension $4N \times 4N$ to be solved, by means of the aggregated space technique. The adjoint error E_p takes only $N = 20$ to reach such a threshold.

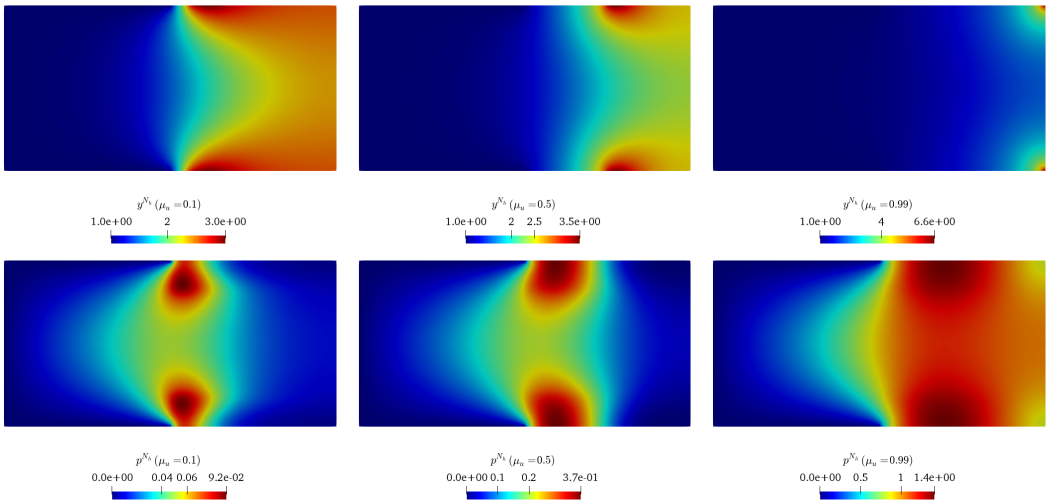

Figure 5. (Test 1: POD). Some high-fidelity solutions for fixed physical parameters ($\mu_1 = 12, \mu_2 = 2.5$) and varying $\mu_u = 0.1, 0.5, 0.99$, from left to right. The state solutions and the adjoint ones are represented on the top and on the bottom of the Figure, respectively.

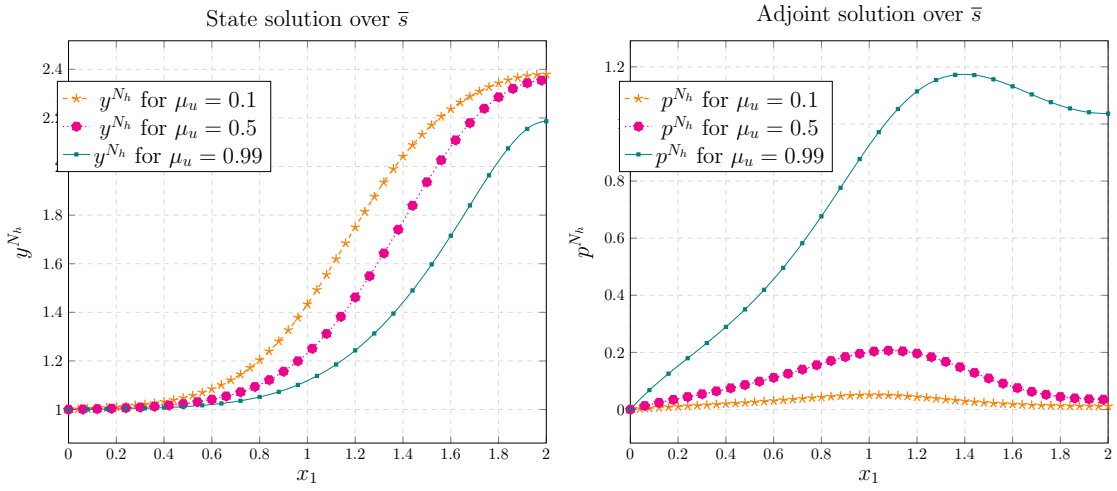

Figure 6. (Test 1: POD). *Left.* State solution y^{N_h} for fixed physical parameters $\mu_1 = 12$ and $\mu_2 = 2.5$ and varying $\mu_u \in \{0.1, 0.5, 0.99\}$ over the segment $\overline{s} = [0, 2] \times \{0.5\}$. *Right.* Analogous representation for the adjoint solution.

This behaviour is not unexpected if one looks at the eigenvalue decay related to the POD modes, depicted in Figure 4 (right plot). It is clear that the POD modes are struggling in representing the state variable, that has a slower decay of the eigenvalues with respect to the adjoint variable. The reason is clearer if we look at Figure 5. We fix the physical parameters to $\mu_1 = 12$ and $\mu_2 = 2.5$ and we study the behaviour of the solution with respect the "vanishing" action of the control, represented in this case by $\mu_u \in \{0.1, 0.5, 0.99\}$, from left to right. The top plots describe the state solution y^{N_h}. Here, we can observe that changing $\Gamma_C^{\mu_u}$ causes a *transportation* of the temperature fields. On the upper and lower boundaries, we see a peak due to the action of the control that heats the system. As one can see, the peak magnitude increases and shifts from left to right. The transport issue is verified by the left plot of Figure 6, too: it represents y^{N_h} over the segment $\overline{s} = [0, 2] \times \{0.5\}$. Also in this case we fix $\mu_1 = 12$ and $\mu_2 = 2.5$ and $\mu_u \in \{0.1, 0.5.0.99\}$. From the plot we see the solution

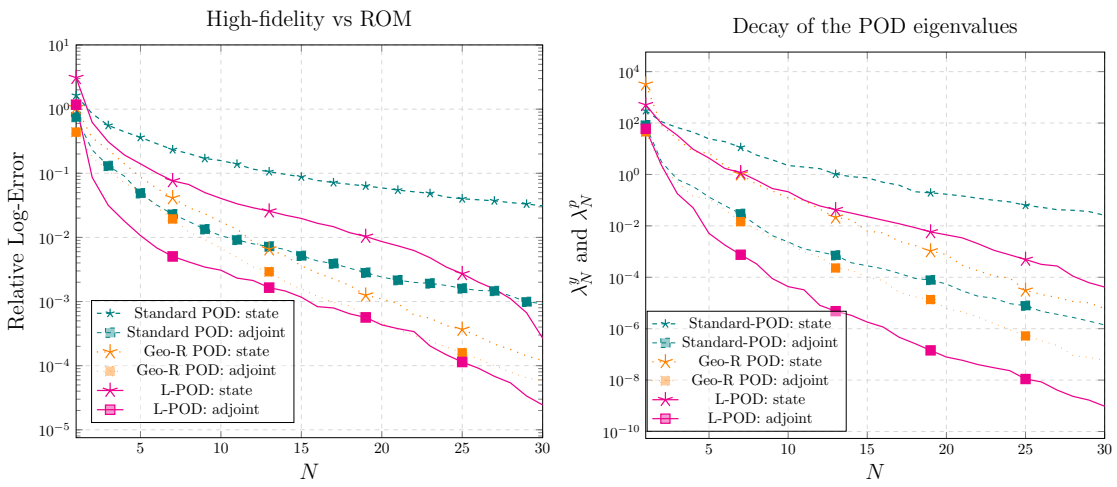

Figure 7. (Test 1: approaches comparison). *Left.* Averaged relative log-error for the two variables for all the approaches. *Right.* Decay of the eigenvalues for the two variables for all the approaches.

moving and transporting itself along the x_1-axis almost unchanged. This behaviour is expected for all the points in $\Omega_2 \cup \Omega_{\text{obs}}$. This is not the case for the adjoint solution (compare the bottom plots of Figure 5 and the right plot of Figure 6).

Namely, letting the control boundary $\Gamma_C^{\mu_u}$ change makes the problem a very difficult task to tackle with standard POD (and in general with ROM, as we specified in Section 3.2). This is confirmed also from the fact that in [44, 57, 77, 78], works where the control boundary was fixed, a few basis functions were necessary to represent the whole phenomenon. The real issue is the moving boundary. We tried two ways to overcome this problem: (i) the L-POD and (ii) the Geo-R. In the following we compare the results of the approaches.

4.1.1. *L-POD.* The L-POD approach, as specified in Section 3.5, is capable to reach more accurate results with respect to the high-fidelity approximation. The setting is the same proposed for the standard POD. We recall that $\boldsymbol{\mu} := (\mu_1, \mu_2, \mu_u) \in \mathcal{P} = (6.0, 20.0) \times (0.5, 3.0) \times (0.0, 1.0)$ and $\alpha = 0.07$. Also in this case, the affine decomposition is recovered by means of a DEIM strategy applied over 350 uniformly distributed parameters. The DEIM is applied with a tolerance of 10^{-5} over the eigenvalue decay and leads to 79 basis functions (this number may not coincide with the standard POD since the 350 parameters are different with respect to the ones used in the standard POD). We stress that the DEIM is applied globally, for all the parametric space $\mathcal{P}$. We exploit Algorithm 1. We set the maximum number of iteration $M = 10$ and $\tau = 10^{-3}$ with $N = 30$. We computed 300 snapshots and they are collected in the $J = 4$ groups determined by the adaptive algorithm. Namely, we did not reach the value of M and I_{μ_u} is partitioned as follows:

$$I_{\mu_u} = (0, 0.25] \cup (0.25, 0.5] \cup (0.5, 0.75] \cup (0.75, 1).$$

Thanks to the application of four separate PODs, we were able to provide (locally), a faster decay of the eigenvalues.

In the right plot of Figure 7, we show the decay of the averaged eigenvalues $\bar{\lambda}_n^y$ and $\bar{\lambda}_n^p$ for $n = 1, \dots, N$, defined, in the setting of L-POD, as

$$\bar{\lambda}_n^y = \frac{1}{J} \sum_{j=1}^{J} \lambda_n^{y\,j} \text{ and } \bar{\lambda}_n^p = \frac{1}{J} \sum_{j=1}^{J} \lambda_n^{p\,j}. \tag{24}$$

For $N = 30$, the L-POD eigenvalues are two orders of magnitude smaller than the ones related to standard POD, both for state and adjoint variables. Finally, the state eigenvalues decay is faster for Geo-R with respect to L-POD, while the adjoint eigenvalues have an opposite behaviour. This

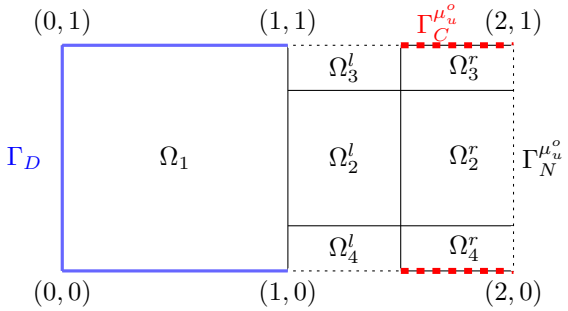

Figure 8. (Test 1). Domain Ω_o for $\mu_u^o = 0.5$. *Observation domain:* $\Omega_{\text{obs}} = \Omega_3^l \cup \Omega_3^r \cup \Omega_4^l \cup \Omega_4^r$, *Control domain:* $\Gamma_C^{\mu_u^o}$ (red dashed line). *Blue solid line:* Dirichlet boundary conditions. *Black dotted line:* Neumann boundary conditions.

reflects onto the average error over 150 uniformly distributed parameters depicted in the left plot of Figure 7. Each $\boldsymbol{\mu}$ in the online phase is sorted in the respective sub-interval and the respective POD basis are used for the Galerkin projection. This local reconstruction gives very accurate results: for $N = 30$, $E_y \sim 2 \cdot 10^{-3}$ and $E_p \sim 2 \cdot 10^{-4}$. We stress that the standard POD is not capable to reach these values neither with $N = 80$. We postpone the comparison between the L-POD and Geo-R relative errors in the next section.

4.1.2. *Geo-R.* As described in Section 3.6, we are going to solve the vbOCP($\boldsymbol{\mu}$) in a reference domain Ω_o. We recall that in the examples usually proposed in literature, the control was "fixed" and the geometrical parameter did not change its nature as in our case.

In Figure 8 we show the geometrical domain used in the Geo-R framework. Here, we consider, once again, $\boldsymbol{\mu} := (\mu_1, \mu_2, \mu_u) \in \mathcal{P} = [6.0, 20.0] \times [1.0, 3.0] \times (0, 1)$. The fixed configuration Ω_o refers to the spatial domain Ω of Figure 3 for a reference parameter $\mu_u^o = 0.5$: we choose the middle point as the most representative case.

In the Geo-R framework, a new mesh was used, thus, in this case, the high-fidelity fidelity dimension is $2N_h = 10356$. The POD is performed in the reference framework over a uniformly distributed training set of 100 samples. Indeed, the problem is simpler and less snapshots can be explored to reach good results. Defining the vector of coordinates in the reference domain as $\mathbf{x}_o = [x_1^o, x_2^o]$, the affine map $T_{\mu_u} : \Omega_o \to \Omega$ is explicitly defined as follows:

$$T_{\mu_u}(\mathbf{x}_o) = \mathbf{x} = \begin{cases} \mathbf{x}_o & \text{in } \Omega_1, \\ \begin{bmatrix} (1 + 2(\mu_u - 0.5))(x_1^o - 1) + 1 \\ x_2^o \end{bmatrix} & \text{in } \Omega_i^l, i = 2, 3, 4, \\ \begin{bmatrix} (1 - 2(\mu_u - 0.5))(x_1^o - 2) + 2 \\ x_2^o \end{bmatrix} & \text{in } \Omega_i^r, i = 2, 3, 4. \end{cases} \tag{25}$$

It is clear that the map T_{μ_u} verifies the assumptions of Section 3.6 and thus the optimization problem can be solved in this new reference domain with numerous benefits.
Indeed, solving the problem in Ω_o allows the state eigenvalues to decay faster than those of the standard POD, as one can see from the right plot of Figure 7. Consequently, the average relative error is capable to reach values around 10^{-4} for both the variables with only $N = 30$, as depicted in the left plot of Figure 7. This result outperforms the standard POD. With respect to L-POD, the state variable is better recovered, while L-POD better reconstructs the adjoint variable up to $N = 15$: above that value, the two approaches are totally comparable.

Concluding:

- standard POD combined with hyper-reduction techniques is an accurate, yet time consuming, way to solve vbOCP($\boldsymbol{\mu}$)s. Indeed, a critical amount of basis functions should be used to

Table 1. Comparison of POD, L-POD and Geo-R in terms of offline computational costs and speed-up.

Strategy	Offline Costs (time in seconds)	Speed-up
POD	935.94s (DEIM $\sim$ 668s)	6
L-POD	1011.49s (DEIM $\sim$ 668s)	17
Geo-R	68.35s (NO DEIM needed)	92

recover a good representation of the high-fidelity solution. However, no issues are encountered for the adjoint variable.

- The L-POD helps in reaching accurate results in the online stage. The strength of this strategy is its versatility. It can be applied to every problem one is dealing with. However, it still relies on hyper-reduction techniques as DEIM.
- A valid option is to recast the problem into an affine decomposed system through Geo-R. Indeed, it allows one to reach more accurate results in a smaller amount of time. The drawback is related to the choice of the reference domain and of the transformation T_{μ_u}. In our case, the choice is made *a posteriori* once observing the physical behaviour of the optimal solutions. We stress that other maps and transformations can be employed. However, this technique can be hardly applied to more complicated geometries.

Remark 2. *We remark that, in our parametric setting, the Geo-R strategy is morally equivalent to the Arbitrary Lagrangian Eulerian formulation proposed in* [81]*. The reference problem aligns the wave-like phenomenon in the center of the domain and builds a low-dimensional framework eliminating the nonlinear features of the solution manifold. For the sake of completeness, we want to stress that we also tried the* shifted-POD *approach proposed in* [58]*. Despite the promising results they obtain for fluid-structure interaction problems, in our specific context, the performances of the strategy in terms of accuracy were disappointing. We noticed large errors when we studied limit cases, i.e.,* $\mu_u \to 0$ *and* $\mu_u \to 1$*. This phenomenon was possibly related to interpolation errors and to the naive shift map we used: it aligned the peak at* $\mu_u = 0.5$ *and extends the solution with the same values along the shifted side. This choice was natural. Nevertheless, it creates fictitious information on the behaviour of the solution and might compromise the accuracy of the ROM solver. For this reason we decide not to show the results and we strongly believe that a deeper analysis of such an approach is needed for vbOCP($\boldsymbol{\mu}$). However, this is beyond the scope of this contribution.*

We stress that the Geo-R allows an affine decomposition of the system and thus and efficient offline-online decoupling of the process. The *speed-up index*, i.e. the number of reduced problem one can perform in the time of high-fidelity solution is around 92, while for the standard POD with $N = 80$, after the DEIM approximation, the speed-up index is 6. The Geo-R approach is more convenient also with respect to the L-POD: indeed with the same value of $N = 30$, L-POD features a speed-up of 17 (the DEIM approach in the online phase affects on the computational performances). Moreover, the advantages of using Geo-R approach for simple geometries is also highlighted from the offline computational costs, since no DEIM is needed in the recast framework. We underline that the small offline cost is also due to the fact that only 100 snapshots are employed in the GEO-R context. We refer the reader to Table 1 for a recap on the computational times. We stress that, as expected, even if L-POD has larger offline costs with respect to standard POD, they are still acceptable and lead to more accurate and faster results in the online phase.

4.2. **Test Case 2: POD and L-POD over a complex geometry.** Despite its capabilities, the Geo-R approach cannot be applied in more complicated settings and it is strictly problem dependent. Therefore, we propose here a case test where no Geo-R can be employed. This test is of interest for real-life applications, since the vbOCP($\boldsymbol{\mu}$)s can be related to the simulation of systems characterized by complex geometries, as we said in the Introduction. The governing PDE($\boldsymbol{\mu}$) is always equation (23).

The spatial domain is represented in Figure 9. We define Γ_{ib} as the boundary of the *dolphin hole* in a unit square geometry[1]. In this test case, $\Gamma_C^{\mu_u} \subset \Gamma_{ib}$. A homogeneous Neumann condition is imposed on the right border of the square and Dirichlet boundary conditions are applied on the other external boundary of the unit square domain. The parameter is $\boldsymbol{\mu} := (\mu_1, \mu_2, \mu_u) \in \mathcal{P} = [6.0, 20.0] \times [0.5, 3.0] \times (0.27, 0.74)$. The parameter μ_1 represents the Péclet number and μ_2 describes the desired constant state. This time, the observation is taken all over the domain. The parameter μ_u ranges from the minimum and the maximum x_1 values of Γ_{ib}. For this test case, $\Gamma_C^{\mu_u} = ((\mu_u, 0.74) \times [0, 1]) \cap \Gamma_{ib}$ and $\Gamma_N^{\mu_u} = (\Gamma_{ib} \setminus \Gamma_C^{\mu_u}) \cup (\{1\} \times [0, 1])$. We set the penalization parameter as the previous experiment: $\alpha = 0.07$.

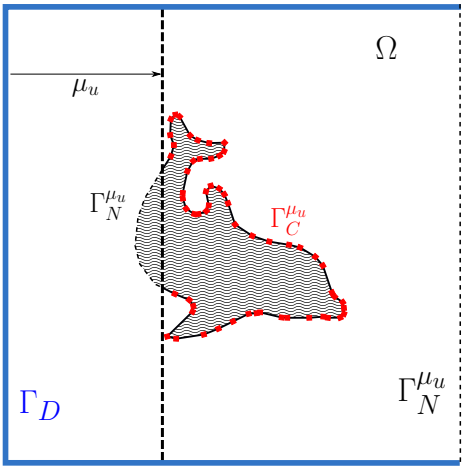

Figure 9. (Test 2). Domain Ω. *Observation domain:* $\Omega_{\text{obs}} = \Omega$, *Control domain:* $\Gamma_C^{\mu_u}$ (red dots). *Blue line:* Dirichlet boundary conditions. *Thin black dashed line:* Neumann boundary conditions. We represent the domain for $\mu_u = 0.33$.

Let us focus on the POD performances. In order to recover the affine decomposition we exploited a DEIM approximation over 350 uniformly distributed parameters to reach a tolerance of 10^{-5} for the eigenvalue decay (i.e. 170 DEIM basis). The POD algorithm is ran over another 300 uniform distributed snapshots. The high-fidelity system is tackled through a $\mathbb{P}^1 - \mathbb{P}^1$ approximation of dimension $2N_h = 5736$. Figure 10 (left plot) shows the relative errors E_y and E_p averaged over a testing set of 150 uniformly distributed parameters in $\mathcal{P}$. The complexity of the problem is visible from the plot. Indeed, 80 basis functions are not enough to reach an accurate state representation, with $E_y \sim 10^{-2}$. While $E_p \sim 10^{-3}$ already for $N = 30$. The claim is confirmed by the decay of the eigenvalues represented in the right plot of Figure 10, which is faster for the adjoint variable.
The main features of the problem can be observed in the plots of Figure 11: we have multiple "peaks" around the dolphin for small values of μ_u and they transfer from left to right for the state variable, while the adjoint variable features a very complex behaviour. In this case, there is no symmetry and the geometrical properties are too complex to perform Geo-R. However, we employ L-POD also in this case. As in the previous test case, we built a global DEIM approximation to recover the affinity assumption. As usual, we used 350 uniformly distributed parameters with the usual tolerance of 10^{-5}. The basis number of the DEIM approximation is 168 (different from the standard POD since the 350 parameters for the hyper-reduction are different from the ones of the standard POD). We run algorithm 1 with $M = 10$, $\tau = 10^{-3}$ and $N = 30$: the interval I_{μ_u} is divided in $J = 7$ sub-intervals as

$$I_{\mu_u} = \bigcup_{i=1}^{J} I_{\mu_u}^i,$$

[1]We are deeply thankful to the contributors who provided this specific geometry which is open access to the following link https://fenicsproject.org/pub/data/meshes/dolfin_fine.xml.

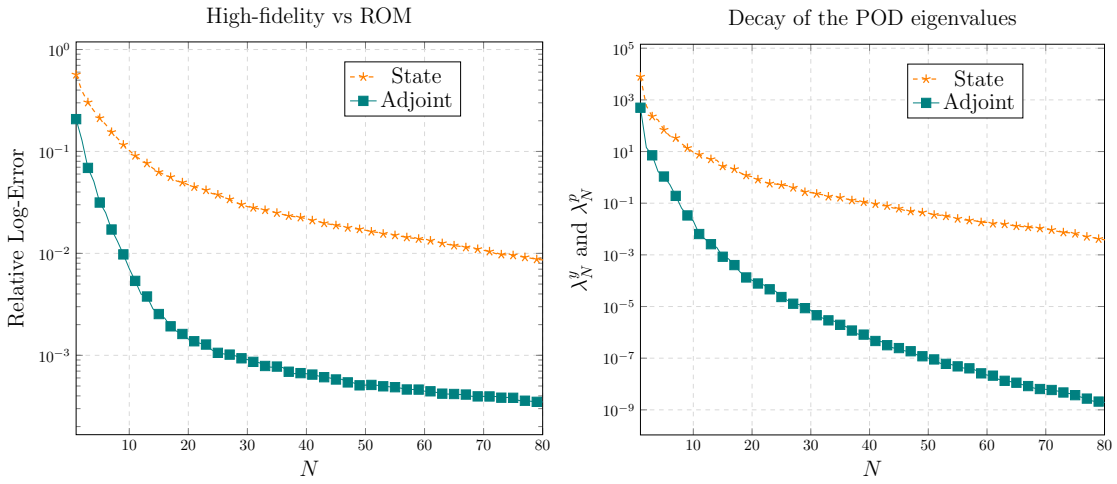

Figure 10. (Test 2: POD). *Left.* Averaged relative log-error for the two variables. *Right.* Decay of the eigenvalues for the two variables.

where $I^1_{\mu_u} = (0.27, 0.32875], I^2_{\mu_u} = (0.32875, 0.3875], I^3_{\mu_u} = (0.3875, 0.44635], I^4_{\mu_u} = (0.44635, 0.505]$, $I^5_{\mu_u} = (0.505, 0.6225], I^6_{\mu_u} = (0.6225, 0.68125]$ and $I^7_{\mu_u} = (0.68125, 0.74)$.

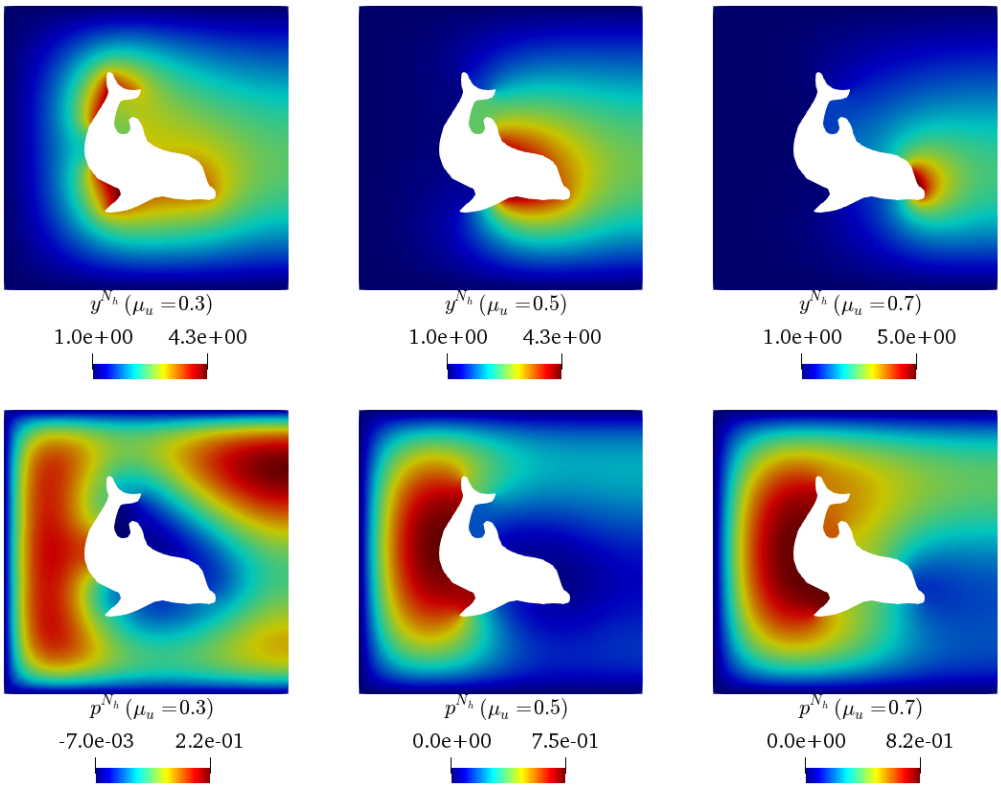

Figure 11. (Test 2: POD). Some high-fidelity solutions for fixed physical parameters ($\mu_1 = 12, \mu_2 = 2.5$) and varying $\mu_u \in \{0.3, 0.5, 0.7\}$, from left to right. The state solutions and the adjoint ones are represented on the top and on the bottom of the Figure, respectively.

Table 2. Comparison of POD and L-POD in terms of offline computational costs and speed-up.

Strategy	Offline Costs (time in seconds)	Speed-up
POD	1844.84 (DEIM $\sim$ 1247s)	2
L-POD	1941.68s (DEIM $\sim$ 1247s)	9

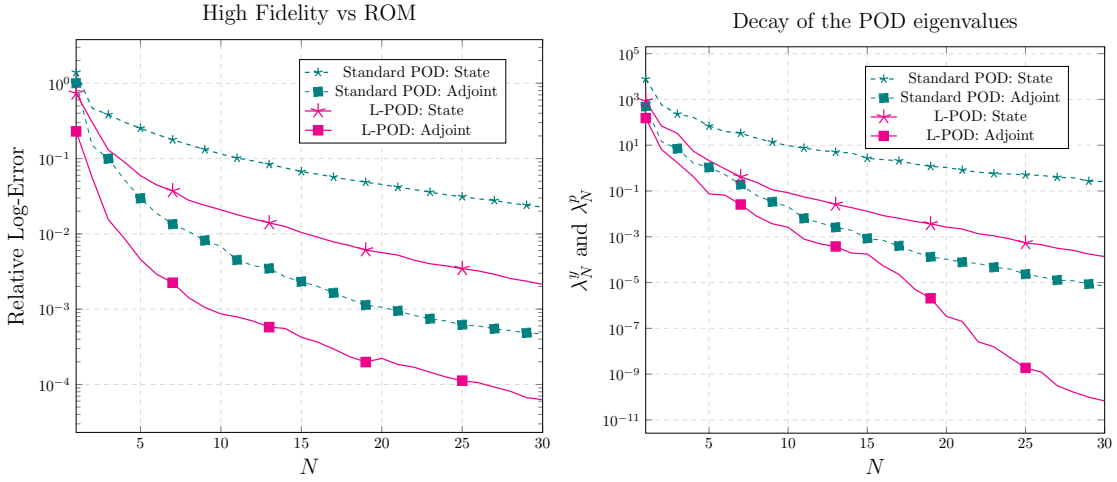

Figure 12. (Test 2: approach comparison). *Left.* Averaged relative log-error for the two variables for all the approaches. *Right.* Decay of the eigenvalues for the two variables for all the approaches.

Thanks to the local approach, if we look at the average eigenvalues in the right plot of Figure 12, we can observe a better behaviour for both the variables. For this reason, the averaged errors on 150 uniformed distributed parameters is lower with respect to standard POD. With L-POD we reach $E_y \sim 2 \cdot 10^{-3}$ and $E_p \sim 7 \cdot 10^{-5}$, as depicted in the left plot of Figure 12. We stress that neither $N = 80$ suffices to reach these values of the relative errors. With a comparable offline phase, the L-POD is also convenient in terms of online costs, with a speed-up around 9. The standard POD features a speed-up of only 2 using $N = 80$. We stress that with comparable online costs, i.e. for $N = 30$, L-POD outperforms standard POD in accuracy. We recap the computational times in Table 2.

5. Conclusions

In this work we deal with ROM techniques to deal with vbOCP($\boldsymbol{\mu}$)s, i.e. boundary optimal control problems where the geometrical action of the control is related to a parameter. Namely, a specific parameter changes the portion of the Neumann boundary where the control plays a role. To the best of our knowledge, it is the first time that this kind of parametric optimal control problem is investigated.

The problem turned out to be difficult to be reduced, since features very complex parametric behaviours. Moreover, the vbOCP($\boldsymbol{\mu}$)s does not verify the affine assumption. We recover it by means of a DEIM algorithm when needed. Guided by the numerical results, we propose tailored approaches inspired by classical methods used in wave-like phenomena and we compared them to standard POD: the Geo-R and the L-POD. The advantages of such strategies have been tested on two numerical experiments: a vbOCP($\boldsymbol{\mu}$) over a simple geometry (where the Geo-R can be applied) and a vbOCP($\boldsymbol{\mu}$) over a complex one (where only L-POD can be performed and compared to standard POD). The proposed tailored strategies outperform standard POD.

We observe that the reduction of vbOCP($\boldsymbol{\mu}$)s is a though task due to the transportation of "peaks" arising for the control action. The diversity of the behaviour of snapshots does not allow a good representation of the physical phenomenon with an acceptable number of basis functions with standard POD technique. In simple cases, one can rely on Geo-R approximation to tackle a simpler problem, where the control boundary is fixed and thus good performances with a smaller amount of basis are guaranteed. Geo-R guarantees good speed-up results, due to the affine structure of the reference problem. However the choice of the reference domain and the map T_{μ_u} is strictly problem dependent and made *a posteriori* once observed the problem at hand. To overcome this limitation, L-POD can be employed. Indeed, L-POD gives more accurate results with respect to standard POD not paying much effort in the offline computation phase. This approach is very general and can be applied to complicated problems characterized by high complex geometries. We stress that L-POD still needs hyper-reduction techniques, as standard POD. However, L-POD is beneficial since it recovers the solution variables more accurately with respect to standard POD for the same values of N (i.e. for online comparable computational costs).

This contribution is a first step towards many further developments. A possible advance is represented by the analysis of error certification for this specific optimal control formulation. Indeed, the problem complies with the error analysis proposed in [57] and [78], however, it suffers large estimator values for the limit case scenarios. Thus, an investigation of a tailored certification can be important for this particular application.

A further interesting advancement would be the analysis of 3D complex geometries. We are aware that the adaptive L-POD strategy (even if generalizable to 3D structures) might suffer higher geometrical complexity resulting in many reduced subspaces and many basis functions to deal with. We are confident that intrusive ROM strategies enhanced by cutting-edge techniques (based on machine learning, for example) might be helpful in this context.

Nevertheless, we believe that the present contribution paves the way to some interesting applications in interdisciplinary fields as geophysics, faults and fractures analysis and energy engineering where the need of fast and reliable simulations for forecast intents is daily increasing.

Acknowledgements

The computations in this work have been performed with RBniCS [1] library, developed at SISSA mathLab, which is an implementation in FEniCS [50] of several reduced order modelling techniques; we acknowledge developers and contributors to both libraries. Computational resources were partially provided by HPC@POLITO, a project of Academic Computing within the Department of Control and Computer Engineering at the Politecnico di Torino (http://hpc.polito.it). This work is partially supported by the INdAM-GNCS project "Metodi numerici per lo studio di strutture geometriche parametriche complesse" (CUP_E53C22001930001) and by the MIUR project "Dipartimenti di Eccellenza 2018-2022" (CUP E11G18000350001).

References

[1] RBniCS – reduced order modelling in FEniCS, http://mathlab.sissa.it/rbnics.

[2] D. Amsallem and B. Haasdonk. Pebl-rom: Projection-error based local reduced-order models. *Advanced Modeling and Simulation in Engineering Sciences*, 3(1), 2016.

[3] D. Amsallem, M. J. Zahr, and C. Farhat. Nonlinear model order reduction based on local reduced-order bases. *International Journal for Numerical Methods in Engineering*, 92(10):891–916, 2012.

[4] I. Babuška. Error-bounds for finite element method. *Numerische Mathematik*, 16(4):322–333, Jan 1971.

[5] E. Bader, M. Kärcher, M. A. Grepl, and K. Veroy. Certified reduced basis methods for parametrized distributed elliptic optimal control problems with control constraints. *SIAM Journal on Scientific Computing*, 38(6):A3921–A3946, 2016.

[6] E. Bader, M. Kärcher, M. A. Grepl, and K. Veroy-Grepl. A certified reduced basis approach for parametrized linear-quadratic optimal control problems with control constraints. *IFAC-PapersOnLine*, 48(1):719–720, 2015.

[7] F. Ballarin, G. Rozza, and M. Strazzullo. Chapter 9 - Space-time POD-galerkin approach for parametric flow control. In E. Trèlat and E. Zuazua, editors, *Numerical Control: Part A*, volume 23 of *Handbook of Numerical Analysis*, pages 307–338. Elsevier, 2022.

[8] M. Barrault, Y. Maday, N. C. Nguyen, and A. T. Patera. An Empirical Interpolation Method: application to efficient reduced-basis discretization of partial differential equations. *Comptes Rendus Mathematique*, 339(9):667–672, 2004.

[9] M. Barrault, Y. Maday, N. C. Nguyen, and A. T. Patera. An 'empirical interpolation' method: application to efficient reduced-basis discretization of partial differential equations. *Comptes Rendus Mathematique*, 339(9):667–672, 2004.

[10] M. Benzi, G. H. Golub, and J. Liesen. Numerical solution of saddle point problems. *Acta Numerica*, 14:1–137, 2005.

[11] S. Berrone, C. Canuto, S. Pieraccini, and S. Scialò. Uncertainty quantification in discrete fracture network models: Stochastic geometry. *Water Resources Research*, 54(2):1338–1352, 2018.

[12] S. Berrone, C. Fidelibus, S. Pieraccini, S. Scialò, and F. Vicini. Unsteady advection-diffusion simulations in complex discrete fracture networks with an optimization approach. *Journal of Hydrology*, 566:332–345, 2018.

[13] N. Biçer, T. Engin, H. Yaşar, E. Büyükkaya, A. Aydın, and A. Topuz. Design optimization of a shell-and-tube heat exchanger with novel three-zonal baffle by using cfd and taguchi method. *International Journal of Thermal Sciences*, 155:106417, 2020.

[14] J. Borggaard, Z. Wang, and L. Zietsman. A goal-oriented reduced-order modeling approach for nonlinear systems. *Computers and Mathematics with Applications*, 71(11):2155–2169, 2016.

[15] F. Brezzi. On the existence, uniqueness and approximation of saddle-point problems arising from lagrangian multipliers. *ESAIM: Mathematical Modelling and Numerical Analysis - Modélisation Mathématique et Analyse Numérique*, 8(R2):129–151, 1974.

[16] J. Burkardt, M. Gunzburger, and H. Lee. POD and CVT-based reduced-order modeling of Navier–Stokes flows. *Computer Methods in Applied Mechanics and Engineering*, 196(1-3):337–355, 2006.

[17] N. Cagniart, Y. Maday, and B. Stamm. Model order reduction for problems with large convection effects. *Computational Methods in Applied Sciences*, 47:131–150, 2019.

[18] G. Carere, M. Strazzullo, F. Ballarin, G. Rozza, and R. Stevenson. A weighted POD-reduction approach for parametrized PDE-constrained optimal control problems with random inputs and applications to environmental sciences. *Computers & Mathematics with Applications*, 102:261–276, 2021.

[19] D. Chapelle, A. Gariah, P. Moireau, and J. Sainte-Marie. A Galerkin strategy with proper orthogonal decomposition for parameter-dependent problems: Analysis, assessments and applications to parameter estimation. *ESAIM: Mathematical Modelling and Numerical Analysis*, 47(6):1821–1843, 2013.

[20] S. Chaturantabut and D. C. Sorensen. Nonlinear model reduction via discrete empirical interpolation. *SIAM Journal on Scientific Computing*, 32(5):2737–2764, 2010.

[21] L. Dedè. Optimal flow control for Navier-Stokes equations: Drag minimization. *International Journal for Numerical Methods in Fluids*, 55(4):347–366, 2007.

[22] L. Dedè. Reduced basis method and a posteriori error estimation for parametrized linear-quadratic optimal control problems. *SIAM Journal on Scientific Computing*, 32(2):997–1019, 2010.

[23] L. Dedè. Reduced basis method and error estimation for parametrized optimal control problems with control constraints. *Journal of Scientific Computing*, 50(2):287–305, Feb 2012.

[24] L. Dedè. Adaptive and reduced basis method for optimal control problems in environmental applications. PhD thesis, Politecnico di Milano, 2008. Available at http://mox.polimi.it.

[25] M. C. Delfour and J. Zolésio. *Shapes and geometries: metrics, analysis, differential calculus, and optimization*, volume 22. SIAM, Philadelphia, 2011.

[26] M. Dihlmann, M. Drohmann, and B. Haasdonk. Model reduction of parametrized evolution problems using the reduced basis method with adaptive time partitioning. pages 156–167, 2012.

[27] M. Drohmann, B. Haasdonk, and M. Ohlberger. Adaptive reduced basis methods for nonlinear convection–diffusion equations. In *Finite Volumes for Complex Applications VI Problems & Perspectives*, pages 369–377. Springer, 2011.

[28] J. Eftang, D. Knezevic, and A. Patera. An hp certified reduced basis method for parametrized parabolic partial differential equations. *Mathematical and Computer Modelling of Dynamical Systems*, 17(4):395–422, 2011.

[29] J. Eftang, A. Patera, and E. Rønquist. An hp certified reduced basis method for parametrized parabolic partial differential equations. *Lecture Notes in Computational Science and Engineering*, 76 LNCSE:179–187, 2011.

[30] S. Fresca, L. Dede', and A. Manzoni. A comprehensive deep learning-based approach to reduced order modeling of nonlinear time-dependent parametrized pdes. *Journal of Scientific Computing*, 87(2), 2021.

[31] S. Fresca and A. Manzoni. POD-DL-ROM: Enhancing deep learning-based reduced order models for nonlinear parametrized pdes by proper orthogonal decomposition. *Computer Methods in Applied Mechanics and Engineering*, 388, 2022.

[32] A. L. Gerner and K. Veroy. Certified reduced basis methods for parametrized saddle point problems. *SIAM Journal on Scientific Computing*, 34(5):A2812–A2836, 2012.

[33] G. V. Grenkin, A. Y. Chebotarev, A. E. Kovtanyuk, N. D. Botkin, and K.-H. Hoffmann. Boundary optimal control problem of complex heat transfer model. *Journal of Mathematical Analysis and Applications*, 433(2):1243–1260, 2016.

[34] B. Haasdonk, M. Dihlmann, and M. Ohlberger. A training set and multiple bases generation approach for parameterized model reduction based on adaptive grids in parameter space. *Mathematical and Computer Modelling of Dynamical Systems*, 17(4):423–442, 2011.

[35] J. S. Hesthaven, G. Rozza, and B. Stamm. Certified reduced basis methods for parametrized partial differential equations. *SpringerBriefs in Mathematics*, 2015, Springer, Milano.

[36] M. Hinze, M. Köster, and S. Turek. A hierarchical space-time solver for distributed control of the Stokes equation. *Technical Report, SPP1253-16-01*, 2008.

[37] M. Hinze, M. Köster, and S. Turek. A space-time multigrid method for optimal flow control. In *Constrained optimization and optimal control for partial differential equations*, pages 147–170. Springer, 2012.

[38] M. Hinze, R. Pinnau, M. Ulbrich, and S. Ulbrich. *Optimization with PDE constraints*, volume 23. Springer Science & Business Media, Antwerp, 2008.

[39] M. Hinze and S. Volkwein. Proper orthogonal decomposition surrogate models for nonlinear dynamical systems: Error estimates and suboptimal control. In *Dimension Reduction of Large-Scale Systems: Proceedings of a Workshop held in Oberwolfach, Germany, October 19–25, 2003*, pages 261–306. Springer, 2005.

[40] L. Iapichino, S. Ulbrich, and S. Volkwein. Multiobjective pde-constrained optimization using the reduced-basis method. *Adv. Comput. Math.*, 43(5):945–972, Oct. 2017.

[41] A. Iollo and D. Lombardi. Advection modes by optimal mass transfer. *Physical Review E - Statistical, Nonlinear, and Soft Matter Physics*, 89(2), 2014.

[42] C. Jäggli, L. Iapichino, and G. Rozza. An improvement on geometrical parameterizations by transfinite maps. *Comptes Rendus Mathematique*, 352(3):263–268, 2014.

[43] M. Kärcher and M. A. Grepl. A certified reduced basis method for parametrized elliptic optimal control problems. *ESAIM: Control, Optimisation and Calculus of Variations*, 20(2):416–441, 2014.

[44] M. Kärcher, Z. Tokoutsi, M. A. Grepl, and K. Veroy. Certified reduced basis methods for parametrized elliptic optimal control problems with distributed controls. *Journal of Scientific Computing*, 75(1):276–307, 2018.

[45] K. Kunisch and S. Volkwein. Control of the burgers equation by a reduced-order approach using proper orthogonal decomposition. *Journal of Optimization Theory and Applications*, 102(2):345 – 371, 1999.

[46] K. Kunisch and S. Volkwein. Proper orthogonal decomposition for optimality systems. *ESAIM: Mathematical Modelling and Numerical Analysis*, 42(1):1–23, 2008.

[47] T. Lassila, A. Manzoni, A. Quarteroni, and G. Rozza. A reduced computational and geometrical framework for inverse problems in hemodynamics. *International Journal for Numerical Methods in Biomedical Engineering*, 29(7):741–776, 2013.

[48] T. Lassila and G. Rozza. Parametric free-form shape design with pde models and reduced basis method. *Computer Methods in Applied Mechanics and Engineering*, 199(23):1583–1592, 2010.

[49] K. Lee and K. Carlberg. Model reduction of dynamical systems on nonlinear manifolds using deep convolutional autoencoders. *Journal of Computational Physics*, 404, 2020.

[50] A. Logg, K. Mardal, and G. Wells. *Automated Solution of Differential Equations by the Finite Element Method*. Springer-Verlag, Berlin, 2012.

[51] Y. Maday, N. C. Nguyen, A. T. Patera, and S. H. Pau. A general multipurpose interpolation procedure: the magic points. *Communications on Pure and Applied Analysis*, 8(1):383–404, 2009.

[52] Y. Maday and B. Stamm. Locally adaptive greedy approximations for anisotropic parameter reduced basis spaces. *SIAM Journal on Scientific Computing*, 35(6):A2417–A2441, 2013.

[53] B. Mohammadi and O. Pironneau. *Applied shape optimization for fluids*. Oxford University Press, New York, 2010.

[54] J. Nečas. Les méthodes directes en théorie des équations elliptiques. 1967.

[55] F. Negri. Reduced basis method for parametrized optimal control problems governed by PDEs. *Master thesis, Politecnico di Milano*, 2011.

[56] F. Negri, A. Manzoni, and G. Rozza. Reduced basis approximation of parametrized optimal flow control problems for the Stokes equations. *Computers & Mathematics with Applications*, 69(4):319–336, 2015.

[57] F. Negri, G. Rozza, A. Manzoni, and A. Quarteroni. Reduced basis method for parametrized elliptic optimal control problems. *SIAM Journal on Scientific Computing*, 35(5):A2316–A2340, 2013.

[58] M. Nonino, F. Ballarin, G. Rozza, and Y. Maday. Overcoming slowly decaying kolmogorov n-width by transport maps: application to model order reduction of fluid dynamics and fluid–structure interaction problems. *arXiv preprint arXiv:1911.06598*, 2019.

[59] M. Ohlberger and S. Rave. Nonlinear reduced basis approximation of parameterized evolution equations via the method of freezing. *Comptes Rendus Mathematique*, 351(23-24):901–906, 2013.

[60] S. Pagani, A. Manzoni, and A. Quarteroni. Numerical approximation of parametrized problems in cardiac electrophysiology by a local reduced basis method. *Computer Methods in Applied Mechanics and Engineering*, 340:530–558, 2018.

[61] D. Papapicco, N. Demo, M. Girfoglio, G. Stabile, and G. Rozza. The neural network shifted-proper orthogonal decomposition: A machine learning approach for non-linear reduction of hyperbolic equations. *Computer Methods in Applied Mechanics and Engineering*, 392:114687, 2022.

[62] B. Peherstorfer. Model reduction for transport-dominated problems via online adaptive bases and adaptive sampling. *SIAM Journal on Scientific Computing*, 42(5):A2803–A2836, 2020.

[63] F. Pichi, M. Strazzullo, F. Ballarin, and G. Rozza. Driving bifurcating parametrized nonlinear pdes by optimal control strategies: Application to navier-stokes equations with model order reduction. *ESAIM: Mathematical Modelling and Numerical Analysis*, 56(4):1361 – 1400, 2022.

[64] A. Quarteroni, A. Manzoni, and F. Negri. *Reduced basis methods for partial differential equations: an introduction*, volume 92. Springer, 2015.

[65] A. Quarteroni, G. Rozza, L. Dedè, and A. Quaini. Numerical approximation of a control problem for advection-diffusion processes. In *Ceragioli F., Dontchev A., Futura H., Marti K., Pandolfi L. (eds) System Modeling and Optimization. International Federation for Information Processing, CSMO Conference on System Modeling and Optimization*, pages vol 199, 261–273. Springer, Boston, 2005.

[66] A. Quarteroni, G. Rozza, and A. Quaini. Reduced basis methods for optimal control of advection-diffusion problems. In *Advances in Numerical Mathematics*, number CMCS-CONF-2006-003, pages 193–216. RAS and University of Houston, 2007.

[67] A. Quarteroni and A. Valli. *Numerical approximation of partial differential equations*, volume 23. Springer Science & Business Media, Berlin and Heidelberg, 2008.

[68] D. Rim, S. Moe, and R. LeVeque. Transport reversal for model reduction of hyperbolic partial differential equations. *SIAM-ASA Journal on Uncertainty Quantification*, 6(1):118–150, 2018.

[69] F. Romor, G. Stabile, and G. Rozza. Non-linear manifold rom with convolutional autoencoders and reduced over-collocation method. *arXiv preprint arXiv:2203.00360*, 2022.

[70] G. Rozza, D. Huynh, and A. Patera. Reduced basis approximation and a posteriori error estimation for affinely parametrized elliptic coercive partial differential equations: Application to transport and continuum mechanics. *Archives of Computational Methods in Engineering*, 15(3):229–275, 2008.

[71] G. Rozza, D. P. Huynh, and A. Manzoni. Reduced basis approximation and a posteriori error estimation for Stokes flows in parametrized geometries: roles of the inf-sup stability constants. *Numerische Mathematik*, 125(1):115–152, 2013.

[72] G. Rozza, T. Lassila, and A. Manzoni. Reduced basis approximation for shape optimization in thermal flows with a parametrized polynomial geometric map. In J. S. Hesthaven and E. M. Rønquist, editors, *Spectral and High Order Methods for Partial Differential Equations*, pages 307–315, Berlin, Heidelberg, 2011. Springer Berlin Heidelberg.

[73] P. Sandra. Uncertainty quantification analysis in discrete fracture network flow simulations. *International Journal on Geomathematics*, 11:1869–2680, 2020.

[74] M. Stoll and A. Wathen. All-at-once solution of time-dependent PDE-constrained optimization problems. 2010.

[75] M. Stoll and A. Wathen. All-at-once solution of time-dependent Stokes control. *J. Comput. Phys.*, 232(1):498–515, Jan. 2013.

[76] M. Strazzullo, F. Ballarin, R. Mosetti, and G. Rozza. Model reduction for parametrized optimal control problems in environmental marine sciences and engineering. *SIAM Journal on Scientific Computing*, 40(4):B1055–B1079, 2018.

[77] M. Strazzullo, F. Ballarin, and G. Rozza. POD-Galerkin model order reduction for parametrized time dependent linear quadratic optimal control problems in saddle point formulation. *Journal of Scientific Computing*, 83(55), 2020.

[78] M. Strazzullo, F. Ballarin, and G. Rozza. A Certified Reduced Basis method for linear parametrized parabolic optimal control problems in space-time formulation. Submitted, 2021, https://arxiv.org/abs/2103.00460.

[79] M. Strazzullo, F. Ballarin, and G. Rozza. POD-Galerkin model order reduction for parametrized nonlinear time dependent optimal flow control: an application to Shallow Water Equations. *Journal of Numerical Mathematics*, 30(1):63–84, 2022.

[80] T. Taddei. A registration method for model order reduction: Data compression and geometry reduction. *SIAM Journal on Scientific Computing*, 42(2):A997–A1027, 2020.

[81] D. Torlo. Model reduction for advection dominated hyperbolic problems in an ale framework: Offline and online phases. *arXiv preprint arXiv:2003.13735*, 2020.

[82] F. Tröltzsch and S. Volkwein. POD a-posteriori error estimates for linear-quadratic optimal control problems. *Computational Optimization and Applications*, 44(1):83 – 115, 2009.

[83] K. Washabaugh, D. Amsallem, M. Zahr, and C. Farhat. Nonlinear model reduction for cfd problems using local reduced-order bases. In *42nd AIAA Fluid Dynamics Conference and Exhibit*, page 2686, 2012.

[84] H. Yang and A. Veneziani. Efficient estimation of cardiac conductivities via pod-deim model order reduction. *Applied Numerical Mathematics*, 115:180–199, 2017.

[85] C. Yu, T. Cheng, J. Chen, Z. Ren, and M. Zeng. Investigation on thermal-hydraulic performance of parallel-flow shell and tube heat exchanger with a new type of anti-vibration baffle and wire coil using rsm method. *International Journal of Thermal Sciences*, 138:351–366, 2019.

[86] Z. Zainib, F. Ballarin, S. Fremes, P. Triverio, L. Jiménez-Juan, and G. Rozza. Reduced order methods for parametric optimal flow control in coronary bypass grafts, toward patient-specific data assimilation. *International Journal for Numerical Methods in Biomedical Engineering*, page e3367, 2020.

[87] R. Zimmermann, B. Peherstorfer, and K. Willcox. Geometric subspace updates with applications to online adaptive nonlinear model reduction. *SIAM Journal on Matrix Analysis and Applications*, 39(1):234–261, 2018.